

The *Gaia* 20 pc white dwarf sample

M. A. Hollands,^{1*} P.-E. Tremblay,¹ B. T. Gänsicke,¹ N. P. Gentile-Fusillo,¹
S. Toonen²

¹ *Department of Physics, University of Warwick, Coventry CV4 7AL, UK*

² *Anton Pannekoek Institute for Astronomy, University of Amsterdam, 1090 GE Amsterdam, The Netherlands*

Accepted XXX. Received YYY; in original form ZZZ

ABSTRACT

Using *Gaia* DR2 data, we present an up-to-date sample of white dwarfs within 20 pc of the Sun. In total we identified 139 systems in *Gaia* DR2, nine of which are new detections, with the closest of these located at a distance of 13.05 pc. We estimated atmospheric parameters for all stellar remnants based on the *Gaia* parallaxes and photometry. The high precision and completeness of the *Gaia* astrometry allowed us to search for wide binary companions. We re-identified all known binaries where both components have accurate DR2 astrometry, and established the binarity of one of the nine newly identified white dwarfs. No new companions were found to previously known 20 pc white dwarfs. Finally, we estimated the local white dwarf space-density to be $(4.49 \pm 0.38) \times 10^{-3} \text{ pc}^{-3}$, having given careful consideration to the distance-dependent *Gaia* completeness, which misses known objects at short distances, but is close to complete for white dwarfs near 20 pc.

Key words: (stars:) white dwarfs – (stars:) Hertzsprung-Russell and colour-magnitude diagrams – stars: statistics

1 INTRODUCTION

White dwarfs are the progeny of stars with initial masses $\lesssim 8\text{--}10 M_{\odot}$ (García-Berro et al. 1997; Iben et al. 1997; Smartt et al. 2009). The strong correlation between stellar mass and luminosity implies rapidly decreasing main-sequence life times for stars more massive than the Sun (Massey & Meyer 2001), and consequently, the vast majority of stars with $M \gtrsim 1.5 M_{\odot}$ ever formed in the Galaxy have already become white dwarfs. Moreover, due to the steep slope of the initial mass function, most of the present-day white dwarfs descended from $\approx 1.2\text{--}2.5 M_{\odot}$ stars. Consequently, the solar neighbourhood is strongly dominated (≈ 75 percent) by low-mass M and K-type stars (see, e.g., Finch et al. 2014; Henry et al. 2018). The remaining ≈ 25 percent are nearly equally split between white dwarfs and main-sequence G, F and A-type stars.¹ Therefore, a volume-limited sample of the stellar population provides constraints on fundamental stellar evolution owing to the rich variety of spectral types (Giammichele et al. 2012; Limoges et al. 2015; Fuhrmann et al. 2017a), the local star formation history (Winget et al. 1987; Tremblay et al. 2014b), the initial mass function (Tremblay et al. 2016), chemical evolution (Fuhrmann et al. 2017b), and the kinematic properties of the Galactic disk or the halo

(Sion et al. 2014). Moreover, as about half of all stars are members of binaries or higher hierarchical multiples, such a sample also yields insight into the initial distributions of binary mass ratios and orbital separations (Duquennoy & Mayor 1991; Raghavan et al. 2010; Duchêne & Kraus 2013; Tokovinin 2014; Moe & Di Stefano 2017; Fuhrmann et al. 2017c; Toonen et al. 2017). The local sample is also a benchmark for the properties and frequencies of exoplanetary systems around stars and white dwarfs (Koester et al. 2014; Dittmann et al. 2017).

Because of the intrinsic faintness of both white dwarfs and low-mass stars, our knowledge of the complete stellar population is currently limited to ≈ 10 pc. For white dwarfs, Holberg et al. (2002, 2008, 2016) compiled the historic local population from the literature, and in parallel, Subasavage et al. (2007, 2008), Sayres et al. (2012) and Subasavage et al. (2017) pursued a dedicated search for nearby white dwarfs, largely based on using reduced proper motions as a proxy for distance. Both groups concluded that the stellar remnant sample within 13 pc can be considered as being essentially complete. Holberg et al. (2008, 2016) accordingly estimated the local space-density of white dwarfs at $4.8 \pm 0.5 \times 10^{-3} \text{ pc}^{-3}$, corresponding to a mass of $3.3 \pm 0.3 \times 10^{-3} M_{\odot} \text{ pc}^{-3}$ given the mean properties of local remnants (Giammichele et al. 2012). This density is expected to hold for the 20 pc sample since the latter volume is located well within the estimated vertical scale height of the disk even for the youngest local

* E-mail: M.Hollands.1@warwick.ac.uk (MH)

¹ <http://www.recons.org/census.posted.htm>

populations (Wegg & Phinney 2012; Buckner & Froebrich 2014; Joshi et al. 2016). Based on that approximation, the pre-*Gaia* 20 pc white dwarf sample is expected to be about 82–86 percent complete (Tremblay et al. 2014b; Holberg et al. 2016). In comparison, a slightly larger space-density of $5.5 \pm 0.1 \times 10^{-3} \text{ pc}^{-3}$ was estimated using the Sloan Digital Sky Survey sample corrected for completeness (Munn et al. 2017). Besides this small discrepancy, there are independent suggestions that the 20 pc sample may be somewhat less complete than currently assumed. While a small number of single, but so far unconfirmed, nearby white dwarf candidates have been reported (e.g. Reyl   et al. 2006), the identification of white dwarf companions to main-sequence stars is a challenging problem (Ferrario 2012). Holberg et al. (2013) discussed the statistics of spatially resolved white dwarf plus F/G/K-type stars, and commented on the fact that three out of five white dwarfs with $D < 5 \text{ pc}$ are within such binaries. However, even M-type stars can outshine cool white dwarfs, with a number of reported candidate binaries within 20 pc (Delfosse et al. 1999; Mace et al. 2018).

The extreme astrometric precision of the *Gaia* Data Release 2 (DR2) will unambiguously allow the confirmation or refutation of all published single white dwarf candidate members with $D \leq 20 \text{ pc}$, and to potentially identify previously unknown nearby degenerate stars. An accurate distance will also be very powerful in corroborating unresolved white dwarf companions to main-sequence stars via the detection of blue/ultraviolet excess flux. *Gaia* DR2 includes 5D phase-space parameters and colours in the G , G_{BP} , and G_{RP} *Gaia* passbands for a large fraction of sources brighter than $G \simeq 21$ magnitude (Gaia Collaboration et al. 2018a; Lindgren et al. 2018; Evans et al. 2018) with a precision that is already of the order of that expected by the end of the mission. Even so, the relative number of *Gaia* sources with 5- vs. only 2-parameter astrometry begins to fall rapidly for sources fainter than $G \simeq 19 \text{ mag}$ (Gaia Collaboration et al. 2018a, Fig. 2), which is potentially problematic for the very coolest and thus faintest white dwarfs, which can have absolute magnitudes exceeding $G_{\text{abs}} = 17 \text{ mag}$ (e.g. J1251+4404, Gianninas et al. 2015). In this work we therefore focus on the white dwarf population within 20 pc, which ensures we are not biased against even the faintest degenerates. We firstly identify new white dwarfs from the *Gaia* HR diagram (Section 2) and look at the kinematics (Section 3) and binarity of the population (Section 4). We then quantify the *Gaia* selection function and resulting space-density for local white dwarfs, a sample that covers the full sky almost isotropically as well as a wide range of magnitudes and proper motions (Section 5). We present our conclusions in Section 6.

2 THE GAIA 20 PC WHITE DWARF SAMPLE

Reddening does not pose a problem to target selection within 20 pc. Therefore a relatively simple query of the *Gaia* database is sufficient to identify all white dwarfs with full five-parameter astrometric solutions. With the goal to inspect, and define the local white dwarf cooling sequence in the Hertzsprung-Russell diagram (HRD), we began by searching the *Gaia* DR2 source catalogue for all objects with

parallaxes greater than 40 mas, (i.e. $D \leq 25 \text{ pc}$),² resulting in 9284 objects.

We then cross-matched an up-to-date list of 193 confirmed white dwarfs, based on Toonen et al. (2017) with revisions from the recent literature (Holberg et al. 2016; Finch & Zacharias 2016; Kirkpatrick et al. 2016; Tremblay et al. 2017; Subasavage et al. 2017; Finch et al. 2018), with published distance estimates that placed them, within uncertainties, within 20 pc. Applying a *Gaia* parallax cut,³

$$\varpi + 3\sigma_{\varpi} > 50, \quad (1)$$

i.e. including white dwarfs that are within their uncertainties at $D < 20 \text{ pc}$, we recovered 125 previously known 20 pc white dwarfs, indicated by their WD numbers in Table 1 and shown as green dots in Fig. 1. Additionally, 57 white dwarfs of the 193 were found to have distances beyond 20 pc (Table 2) and 11 stellar remnants were either absent in *Gaia* DR2, or did not have full five-parameter astrometry (discussed further in Section 2.3).

These 125 stars were used to define a generous colour cut to select a sub-set of the *Gaia* 20 pc sample that we would scrutinize for so far unknown white dwarfs,

$$G_{\text{abs}} > 9.7 + 4.7 \times (G - G_{\text{RP}}), \quad (2)$$

$$G_{\text{abs}} < 14.7 + 4.7 \times (G - G_{\text{RP}}), \quad (3)$$

$$G - G_{\text{RP}} < 1.1, \quad (4)$$

$$\varpi + 3\sigma_{\varpi} > 50. \quad (5)$$

We use $G - G_{\text{RP}}$ as colour information instead of $G_{\text{BP}} - G_{\text{RP}}$, as very low mass main-sequence stars have poorly defined G_{BP} magnitudes, and consequently scatter into the white dwarf locus in the HRD. The HRD selected with the above cuts contains a large number of objects between the faint ends of the main-sequence and the white dwarf cooling sequence, at suspiciously close distances ($< 5 \text{ pc}$). Inspection of the spatial distribution revealed that the majority of these sources are in the Galactic plane. Given that for the 20 pc sample the spatial distribution should be isotropic demonstrates that these sources correspond to spurious detections. Applying a simple cut on the astrometric noise (ASTROMETRIC_EXCESS_NOISE $< 1 \text{ mas}$) similarly to what has been done in Gaia Collaboration et al. (2018b) removes the majority of these problematic data (flagged with red outlines in Fig. 1). This cut removes, however, one known white dwarf, Sirius B (WD 0642–166). Given that Sirius B is the companion to the brightest known star in the sky apart from the Sun, we believe it is adequate to treat this system differently and add it to our sample.⁴ We have not applied any of the other quality cuts discussed in Gaia Collaboration et al. (2018b). In particular, the suggested cut on VISIBILITY_PERIODS_USED would have removed five known

² For the general case, calculating distances from *Gaia* parallaxes is not trivial (Bailer-Jones 2015; Bailer-Jones et al. 2018). However, for white dwarfs within 20 pc, the fractional parallax uncertainties are sufficiently small that distances and their uncertainties can be accurately calculated according to $D = 1/\varpi$, $\sigma_D = \sigma_{\varpi}/\varpi^2$.

³ We decided to adopt the published parallax zero-point, the 0.03 mas offset discussed by Lindgren et al. (2018) is of the order of the 1σ uncertainty on ϖ for the bulk of the white dwarf sample.

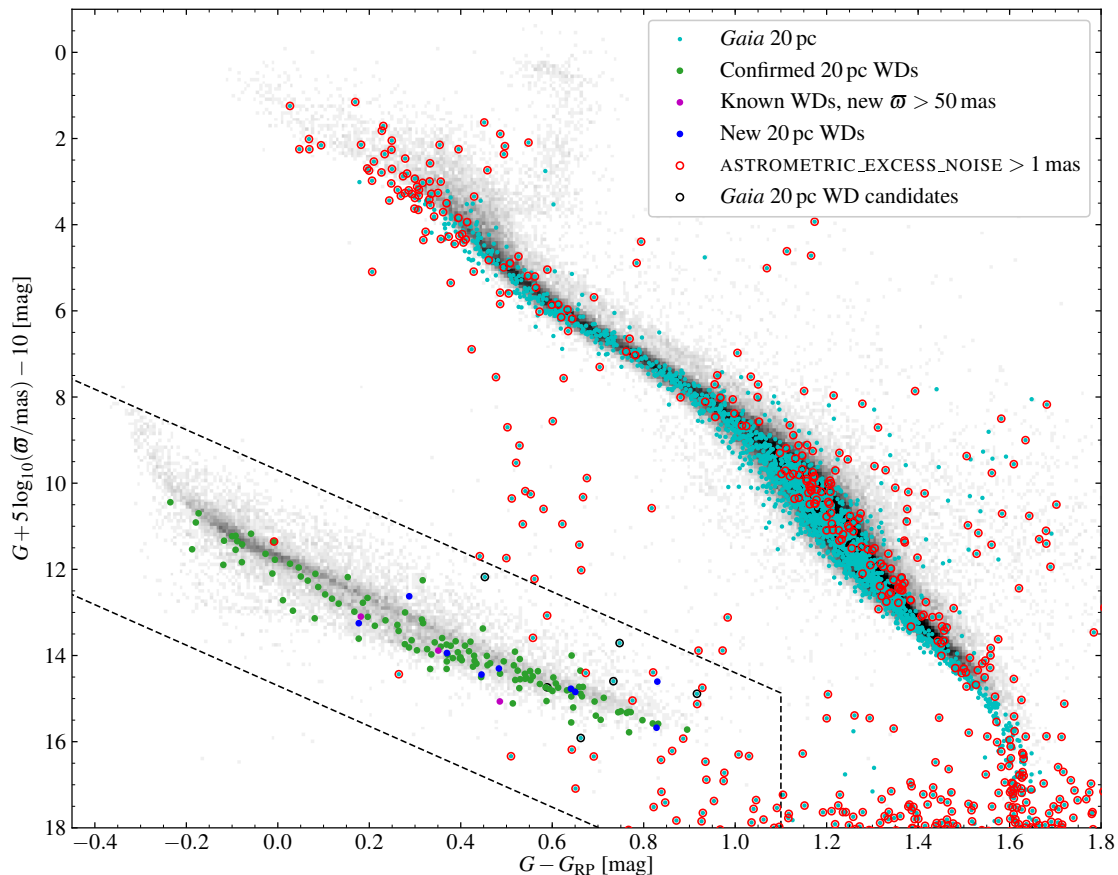


Figure 1. Hertzsprung-Russell diagram of the stellar population within 20 pc detected by *Gaia*, non-degenerate stars are plotted as small turquoise symbols. White dwarfs previously known to be within 20 pc are shown in green, known white dwarfs that the *Gaia* parallax places at $D < 20$ pc in magenta, and newly discovered degenerate stars in blue. The dashed lines show the colour cut used to select white dwarf candidates. *Gaia* sources with `ASTROMETRIC_EXCESS_NOISE` > 1 mas are indicated by red circles – only one known white dwarf (Sirius B) is affected by this. The six rejected white dwarf candidates are shown by black circles, though one of these is partially obscured by known white dwarfs. For guidance, clean main-sequence and white dwarf sequences selected from *Gaia* DR2 are shown in grey.

white dwarfs for which the *Gaia* data agree with ground-based measurements and one new degenerate star.

Removing the 125 known white dwarfs left 20 objects that we inspected individually. Three of them turned out to be known white dwarfs that were not previously considered to be within 20 pc (WD 0959+149: 25.05 ± 0.69 pc, Holberg et al. 2016; WD 1316–215: 31.6 ± 5.3 pc, Subasavage et al. 2007; WD 1350–090: 25.3 ± 1.0 pc, Giammichele et al. 2012). Two more of the 20 were very recent white dwarfs identifications that were missed from our initial list of 193 objects. One (*Gaia* DR2 5867776696271127424) was found as a probable white dwarf by Smith et al. (2018) in the VVV survey, owing to its large reduced-proper motion. The *Gaia* DR2 parallax secures the degenerate nature of this star. The other (*Gaia* DR2 2202703050401536000) was recently identified by Scholz et al. (2018) as a companion to TYC 3980-1081-1, located at a distance of 8.46 pc. For the

remaining 15 objects, we analysed archival photometry and imaging, in particular from Pan-STARRS and 2MASS. The nature of these objects is discussed in detail in Section 2.2, where we conclude that 9 of them are indeed white dwarfs (blue dots in Fig. 1), whereas the final 6 are likely contaminants scattered into the white dwarf sequence in the HRD due to poor photometry and/or astrometry.

2.1 Atmospheric parameters

In order to fully understand the *Gaia* DR2 data set for known white dwarfs and to prepare for the identification of new local remnants in Section 2.2, we estimated the atmospheric parameters of all sources that are included in our cuts given by Equations (1–5). We only employed the measured fluxes in the G , G_{BP} and G_{RP} passbands as well as the parallax as input parameters of our fitting procedure. We have used pure-hydrogen (Tremblay et al. 2011), pure-helium (Bergeron et al. 2011), and mixed model atmospheres (Tremblay et al. 2014a) to calculate the monochromatic surface Eddington flux H_1 as a function of effective tempera-

⁴ Similarly, the Procyon system is absent from *Gaia* DR2 possibly from saturation of the primary, and 40 Eri B is also missing though the A and C components are present in DR2 (see Section 2.3).

ture (T_{eff}) and surface gravity ($\log g$). The mass-radius relations of [Fontaine et al. \(2001\)](#) for thick hydrogen layers ($M_{\text{H}}/M_{\text{WD}} = 10^{-4}$; pure-H atmospheres) and thin hydrogen layers ($M_{\text{H}}/M_{\text{WD}} = 10^{-10}$; pure-He and mixed atmospheres) were employed to compute the stellar flux of the white dwarf as a point source, which was then integrated through the revised *Gaia* DR2 passbands $S(\lambda)$ of [Evans et al. \(2018\)](#) in units of quantum efficiency as

$$F_{\lambda}^m = \frac{\int 4\pi R^2 H_{\lambda}(T_{\text{eff}}, \log g) S^m(\lambda) \lambda d\lambda}{\int S^m(\lambda) \lambda d\lambda}, \quad (6)$$

where m represents a given *Gaia* filter (G , G_{BP} , G_{RP}). The observed quantity is

$$f_{\lambda}^m = \varpi^2 F_{\lambda}^m, \quad (7)$$

where f_{λ}^m is the *Gaia* flux in units of $\text{erg cm}^{-2} \text{s}^{-1}$. To determine the T_{eff} and $\log g$, we minimized the χ^2 between the absolute *Gaia* photometry and absolute synthetic magnitudes calculated from the above models, employing the non-linear least-squares Levenberg-Marquardt algorithm ([Press et al. 1992](#)). The stellar radius, R , in Equation (6) is fully defined by the atmospheric parameters and our adopted mass-radius relation. The uncertainties were directly obtained from the covariance matrix of the fit although these are underestimates, since we did not include the unknown systematic errors of the spectral models, *Gaia* passbands, or mass-radius relations in the χ^2 .

The currently known stellar remnants within 20 pc have a wide variety of atmospheric compositions and spectral types, summarised in Table 1. While the majority of these white dwarfs are thought to have pure hydrogen or pure helium atmospheric compositions, at least 39 percent have a magnetic field, or traces of carbon and other metals. As a consequence, a complete model atmosphere analysis using all available spectroscopy as well as new *Gaia* data would be necessary to provide a physically meaningful update of the atmospheric parameters of previously known white dwarfs. The *Gaia* solutions presented in Table 1 should be taken with caution and serve as a reference to understand atmospheric parameters derived from *Gaia* and the future characterisations of larger *Gaia* samples.

In Fig. 2 we highlight the comparison of our *Gaia* DR2 parameters to previously established values from the literature ([Gianninas et al. 2011](#); [Farihi et al. 2011](#); [Giammichele et al. 2012](#); [Limoges et al. 2015](#); [Subasavage et al. 2017](#)). As much as possible we adopted literature parameters based on photometric rather than spectroscopic estimates for objects with $T_{\text{eff}} < 10\,000$ K allowing for a more direct comparison with *Gaia*. In the case of 1D spectroscopic solutions we corrected for 3D effects ([Tremblay et al. 2013](#)). In all cases *Gaia* DR2 alone can not constrain the atmospheric composition and we adopt in Table 1 the same composition as these earlier analyses. For white dwarfs of unknown spectral types, we assumed a pure-hydrogen composition. Fig. 2 suggests a very good agreement between established and *Gaia* DR2 parameters, even for DQ and DZ white dwarfs (orange), which differ significantly from the pure-helium approximation. This is likely a consequence of the extremely broad *Gaia* passbands and the fact that the sensitivity of atmospheric parameters to *Gaia* colours decreases significantly with temperature. Fig. 3 compares our adopted *Gaia* DR2 parameters with

an analysis that assumed a pure-hydrogen composition for all objects with helium dominated atmospheres. The effect is fairly mild owing to the broad *Gaia* passbands, and it suggests that using the pure-hydrogen approximation for newly discovered *Gaia* white dwarfs provides a fairly reasonable estimate of their atmospheric parameters as long as one is cautious about possible outliers when deriving astrophysical relations.

The precision of the *Gaia* DR2 data is extremely high resulting in similarly small error bars on the atmospheric parameters in Table 1 and Figs. 2–4. It is clear that these error bars are only statistical in nature, and should be taken with some caution, especially considering our approximation on the atmospheric composition. Furthermore, it is unlikely that the accuracy of the physics in the model atmospheres reach the *Gaia* 20 pc sample precision. A much more conservative error estimate for the atmospheric parameters of individual objects can be made by comparing the average deviation between *Gaia* and published parameters. We find deviations of 3.1 percent in T_{eff} and 0.10 dex in $\log g$. This likely overestimates the errors since the *Gaia* data set is more precise and homogeneous than earlier measurements.

The *Gaia* DR2 surface gravity distribution of the 20 pc sample is presented in Fig. 4. It agrees with a sharply peaked distribution centred on the canonical value of $\log g = 8.0$. However, the coolest objects in the sample, adopting the atmospheric composition of published photometric analyses, show a trend towards lower surface gravities. We currently do not know the reason for this behaviour that was also observed by [Gaia Collaboration et al. \(2018b\)](#). In this regime, the effects of collision-induced-absorption and the red-wing of the Ly α line become important for the optical colours ([Borysov et al. 2001](#); [Kowalski & Saumon 2006](#); [Blouin et al. 2017](#)).

2.2 New white dwarfs

The colour cuts of Equations (1–5) and the quality cut on astrometric noise left us with 15 new white dwarfs candidates within 20 pc. The *Gaia* photometric fits performed in Section 2.1 can help to identify the nature of these objects but additional information was needed to separate genuine new white dwarfs from spurious entries in the *Gaia* database. To this aim, we have gathered additional photometry by matching 13 objects with 2MASS ([Skrutskie et al. 2006](#)) and 8 with Pan-STARRS ([Chambers et al. 2016](#)). We have integrated the same model grids as those used in Section 2.1 to calculate synthetic fluxes using the appropriate filters ([Cohen et al. 2003](#); [Tonry et al. 2012](#)). In Appendix A we show all individual fits for 8 objects with both Pan-STARRS and 2MASS, 5 sources with *Gaia* and 2MASS, and 2 stars with *Gaia* data only. For 9 objects we conclude that all available data is consistent with a previously unknown white dwarf, these stars are flagged accordingly in Table 1. The table also includes their estimated atmospheric parameters derived from *Gaia* data alone, consistent with the sample of known white dwarfs. A more detailed assessment of their properties will have to await follow-up spectroscopy. The following stars are worth a special mention:

Gaia DR2 2486388560866377856 is a high-proper motion star (LP 649–66), and has a common proper motion M-dwarf companion (LP 649–67, see Section 4.1). Neither

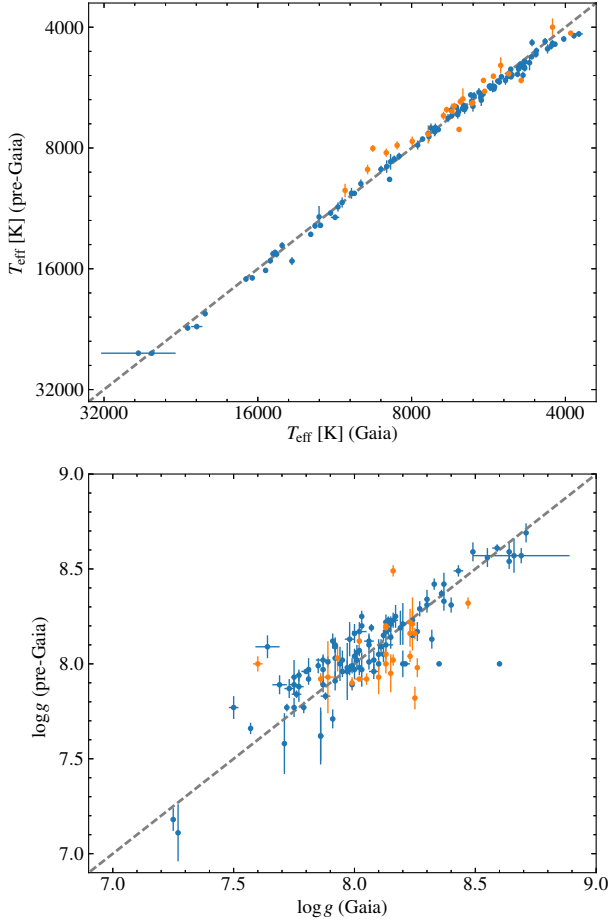


Figure 2. Comparison of published atmospheric parameters and those derived here based on the *Gaia* parallaxes and photometry. DQ and DZ stars are shown in orange with all other objects in blue.

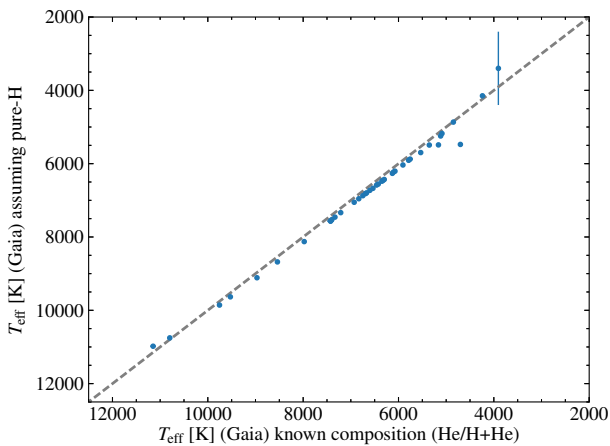


Figure 3. Comparison of the fits to the *Gaia* data assuming a pure-H atmosphere for those objects in Table 1 that are assigned a pure-He or mixed He/H atmosphere.

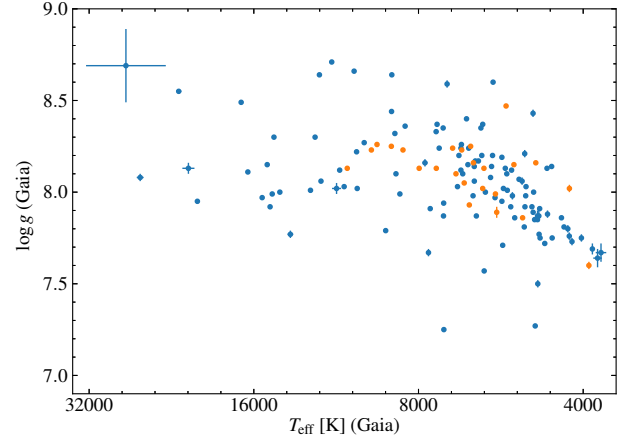


Figure 4. $\log g - T_{\text{eff}}$ distribution of photometric *Gaia* DR2 parameters. The colours of the symbols are the same as in Fig. 2.

Pan-STARRS or 2MASS data are available, but the low luminosity and *Gaia* colours of this source confirm the degenerate nature.

***Gaia* DR2 4970215770740383616** is an outlier in terms of its PHOT_BP_RP_EXCESS_FACTOR value of 1.661, indicating that the modelling of the background flux is poor. This star is a known high-proper motion object (Luyten & Hughes 1980; Platais et al. 1998), which is well-resolved in archival imaging, but moved to within ≈ 1.1 arcsec of a star of nearly identical optical brightness during the epoch of the *Gaia* observations (DR2), which probably explains the poor astrometry. However, considering the high proper motion and the fact that the *Gaia* *G* and *JHK* magnitudes agree with a degenerate star of $T_{\text{eff}} = 5270$ K and $\log g = 8.0$, we conclude that it is likely a new white dwarf. Ground-based follow-up spectroscopy will be challenging for the next few years due to its close proximity to the other star.

***Gaia* DR2 5224999346778496128** is a faint ($G = 17.18$ mag), high-proper motion source, that is neither in 2MASS or Pan-STARRS. It has no *Gaia* flags that would suggest lower quality data hence we consider this object as a very cool white dwarf.

We are left with 6 *Gaia* sources that are unlikely to be white dwarfs which are summarised in Table 3. Five of them have *JHK* flux excesses suggesting a main-sequence star. The average ASTROMETRIC_EXCESS_NOISE parameter for these objects is 0.56 mas, while the average for the new and confirmed 20 pc white dwarf sample is much lower at 0.07 mas. Furthermore, all but one of these objects have VISIBILITY_PERIODS_USED < 8 and hence would not have made the cuts proposed in Gaia Collaboration et al. (2018b). A deeper discussion is required for the rejected object *Gaia* DR2 6206558253342895488. Inspection of its photometric fit (Fig. A2) shows mild disagreement between the *Gaia* and 2MASS photometry. This is most likely contamination from a B-type star situated 16 arcsec away, seeing as the 2MASS contamination flags are raised. Visually, the data resembles WD 2307+548, whose 2MASS photometry is similarly contaminated by its companion. While, on this basis, claiming *Gaia* DR2 6206558253342895488 to be a new white dwarf

is tempting, the accuracy of its astrometry is questionable. The astrometric excess noise is a modest 0.62 mas, however the proper motion is the most suspicious aspect. The *Gaia* data give $(\mu_{\text{Ra}}, \mu_{\text{Dec}}) = (+71.19 \pm 0.82, -54.16 \pm 0.56) \text{ mas yr}^{-1}$, but is found to be $(-36.5 \pm 9.0, -25.3 \pm 9.0) \text{ mas yr}^{-1}$ and $(-74.9 \pm 6.9, -28.0 \pm 6.6) \text{ mas yr}^{-1}$ in the NOMAD (Zacharias et al. 2004) and SPM (Girard et al. 2011) catalogues, respectively. While these two measurements are only marginally consistent with each other, they are both in clear disagreement with the *Gaia* proper motion. Therefore it is reasonable to assume that the *Gaia* parallax of this star is equally unreliable, in which case the object could be a K-type star situated at a much greater distance. A spectroscopic follow-up of the 6 sources identified in Table 3 can help to identify their nature.

2.3 Known missing systems

While *Gaia* DR2 includes the majority of known 20 pc members, eleven white dwarfs known (or thought to be) within 20 pc are missing and are summarised in Table 4.⁵ Of these eleven, the eight with prior parallaxes are all located within 14 pc indicating that non-detection primarily affects the nearest objects. These absences appear to be caused for a variety of reasons. For many of these, high proper motion is the probable culprit where *Gaia* DR2 is estimated to be missing 17 percent of sources with proper motions $> 600 \text{ mas yr}^{-1}$ (Gaia Collaboration et al. 2018a), although this is described as having a greater impact on bright stars. Binary companions can also lead to the non-detections of white dwarfs. In the case of Procyon B (WD 0736+053), no sources are detected within 45 arcsec of the primary. While this could be attributed to saturation of Procyon A, we note that Sirius B is present in the *Gaia* data despite its proximity to the brightest star in the sky. For the 40 Eri system, the white dwarf component (40 Eri B) is missing although the A and C components both have full *Gaia* astrometry. For the WD 0727+482A/B system, the non-detection of both white dwarfs is likely associated with their large astrometric excess noise of $\approx 10 \text{ mas}$, potentially caused by their close binary orbit (their projected separation is $\approx 7 \text{ au}$). The missing systems are analysed further in Section 5, where they are used to constrain the distance-dependent completeness of the *Gaia* stellar remnants within 20 pc.

2.4 Mass distribution

The present day distribution of white dwarf masses encodes the product of multiple astrophysical processes of scientific importance, in particular the initial mass function, star formation history, initial-to-final mass relation (IFMR), and binary interactions such as accretion or mergers (see, e.g.,

⁵ We note in passing LHS 1249, which was discussed by Reylé et al. (2006) as a white dwarf candidate, based on a featureless spectrum (their Fig. 3), with a photometrically estimated distance of 14.4 pc. LHS 1249 is catalogued as an M3-dwarf (Pesch & Sanduleak 1978), which is consistent with the *Gaia* parallax and 2MASS *JHK* photometry. We conclude that LHS 1249 is not a white dwarf, though the spectrum presented by Reylé et al. (2006) remains puzzling.

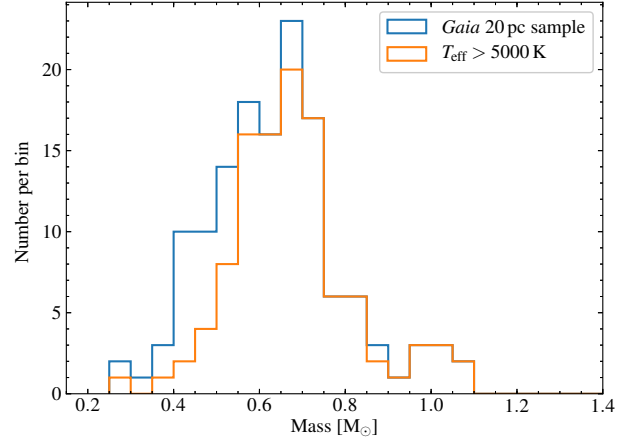


Figure 5. Mass distribution of our sample (blue). The reduced sample of objects with $T_{\text{eff}} > 5000 \text{ K}$ is shown in orange.

Liebert et al. 2005; Giammichele et al. 2012; Tremblay et al. 2014b, 2016; Toonen et al. 2017).

Based on the atmospheric parameters measured from fitting the *Gaia* data, and our adopted M-R relations (Section 2.1), we determined the mass of each white dwarf detected by *Gaia* in the 20 pc sample. In Fig. 5 we show the mass distribution for these stellar remnants (blue). Because Fig. 4 shows a systematic decrease in $\log g$ at low T_{eff} (described in Section 2.1), we therefore present a reduced mass distribution for objects with $T_{\text{eff}} > 5000 \text{ K}$ (orange), which are minimally affected.

Since the release of *Gaia* DR2, Kilic et al. (2018) have also studied the white dwarf mass distribution within a distance of 100 pc. Their much larger sample of $\approx 14\,000$ sources showed a highly bimodal mass distribution, with a highest peak located at the canonical $0.6 M_{\odot}$, plus a broader and weaker peak near $0.8 M_{\odot}$, which Kilic et al. 2018 attributed to mergers.

El-Badry et al. (2018) also analysed white dwarfs within 100 pc for the purpose of constraining the initial-to-final mass relation. They too identified a second peak in the white dwarf mass distribution located at $0.8 M_{\odot}$, though their analysis is limited to objects with $G_{\text{abs}} < 14$. Instead of mergers, El-Badry et al. (2018) attribute this to a flattening in the IFMR for initial masses of $3.5\text{--}5.5 M_{\odot}$.

In contrast with the results of Kilic et al. (2018) and El-Badry et al. (2018), Fig. 5 does not show an excess of objects near $0.8 M_{\odot}$, and instead appears broadly similar to the results presented in other recent work (e.g. Genest-Beaulieu & Bergeron 2014; Rebassa-Mansergas et al. 2015; Kepler et al. 2016; Tremblay et al. 2016). Even considering the relatively small sample size, the bimodal mass distribution found by Kilic et al. (2018) and El-Badry et al. (2018) should be visible in Fig. 5 if present in the 20 pc sample.

3 KINEMATICS

The *Gaia* astrometry includes both parallaxes and proper motions. Thus the tangential velocity, v_{\perp} , can be determined entirely from *Gaia* DR2 data.

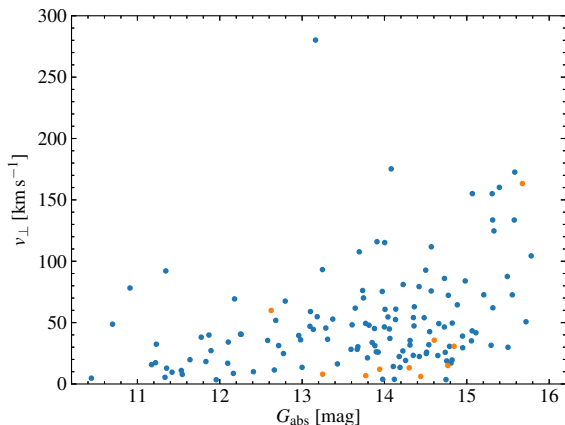


Figure 6. Tangential velocities as a function of absolute G magnitude. The 9 new objects identified in this work are shown in orange.

The tangential velocity is best studied as a function of the total age of a white dwarf including the main-sequence lifetime (see, e.g., Fig. 5 of Tremblay et al. 2014b). Using the white dwarf cooling age (or absolute magnitude) alone, it is difficult to separate Galactic disk white dwarfs into components that possibly have a different scale height (Sion et al. 2014). Nevertheless, a correlation between absolute G magnitude and tangential velocity is expected, as faint local white dwarfs with large cooling ages must have a large total age. We must be cautious, however, since young remnants are a mix of young and old stars of different masses. Fig. 6 shows G_{abs} as a function of tangential velocity and confirms that correlation. All white dwarfs including new detections are consistent with disk kinematics, except possibly for WD 1756+827 with $v_{\perp} = 280 \text{ km s}^{-1}$.

While most *Gaia* white dwarfs lack radial velocity measurements an estimate of the 3D velocity in terms of the U, V, and W Galactic coordinates can help to identify halo candidates (Chiba & Beers 2000). For WD 1756+827, Fuchs & Jahreiß (1998) and Fuhrmann et al. (2012) suggest either halo membership or a high-velocity thick-disc star. WD 1756+827 is a relatively young white dwarf with a cooling age of 1.4 Gyr. However, *Gaia* parameters suggest a mass of $0.52 M_{\odot}$, which is consistent with the value of $0.53 M_{\odot}$ from Limoges et al. (2015), and thus a large main-sequence lifetime.

4 MULTIPLE SYSTEMS

With the arrival of parallaxes for an unprecedented number of stars comes the opportunity to identify new binary/multiple systems, at both close and wide separations. Here we outline our detections of multiple systems identified within the 20 pc white dwarf sample.

4.1 Wide binaries

In the pre-*Gaia* era, a typical approach to identify resolved binaries was to perform a cone-search around one’s target,

and then search for other sources with comparable proper motion. This approach is reasonable in the absence of universal parallaxes, but is restrictive for finding the widest binaries, particularly for stars in the Solar neighbourhood, like those of interest here. For example, a cone-search of a few arcmin might be chosen to avoid selecting too large a number of sources (which could not previously be pre-filtered by parallax), yet on-sky separations of a few degrees are possible in the most extreme cases, where physical separations can approach 1 pc (Caballero 2010).

With the parallaxes provided by *Gaia* DR2, such limitations are relegated to the past (at least for local stars). Instead we perform our companion search in terms of distances and tangential-velocities.

For computational efficiency, we initially limited our search to *Gaia* sources with $\varpi > 40 \text{ mas}$ only. For each white dwarf identified in Section 2, we performed a cone-search scaled by white dwarf distance – in effect a cylindrical search within a projected separation (D_{\perp}) of 1 pc. At 20 pc, this corresponds to an angular-radius of about 3 degrees. We next made a cut on the absolute difference in radial distances (ΔD_{\parallel}) again of 1 pc, but including some leeway for uncertainty, i.e.

$$|\Delta D_{\parallel}| - 3\sigma_{\Delta D_{\parallel}} < 1 \text{ pc}. \quad (8)$$

Thus, for each degenerate star, we searched for companions in a cylindrical volume of $\approx 6.3 \text{ pc}^3$. Finally, for each white dwarf we checked the stars within the search-volume for consistent tangential-velocities, by calculating the velocity differences in km s^{-1} ,

$$\Delta v_{\perp} = 4.7405 \sqrt{(\Delta \mu_{\text{Ra}})^2 + (\Delta \mu_{\text{Dec}})^2} / \varpi_{\text{wd}}, \quad (9)$$

where ϖ_{wd} is the parallax of the white dwarf in mas, and $\Delta \mu_{\text{Ra/Dec}}$ are the differences in the right-ascension/declination components of proper motion in mas yr^{-1} . In Fig. 7, we show Δv_{\perp} against D_{\perp} for all *Gaia* sources found within the search volumes of all 20 pc white dwarfs.⁶ Two prominent distributions are observed – well separated stars with large Δv_{\perp} (blue points), and closer stars with more comparable v_{\perp} . This latter group predominantly consists of known companions to 20 pc white dwarfs, but also a companion to one of the nine newly identified white dwarfs (green point), which is discussed further below. Information regarding all identified wide pairs is also presented in Table 5.

The new wide binary system contains the newly discovered white dwarf *Gaia* DR2 2486388560866377856 (J2015.5 coordinates 02:12:28.34, $-08:04:17.9$), which is located at a distance 16.7 pc. The binarity of this system (LP 649–66/67) was already recognised (Heintz 1993; Luyten 1997), however the white dwarf nature of LP 649–66 has only now been confirmed with *Gaia* data. In SDSS imaging, the white dwarf is only partially resolved from LP 649–67 at a separation of 4 arcsec.

A noteworthy feature of the binary distribution in Fig. 7 is the negative correlation between Δv_{\perp} and D_{\perp} . Because the uncertainties in both dimensions are smaller than the points

⁶ For the abscissae in Fig. 7, D_{\perp} is preferable to either $|\Delta D_{\parallel}|$ or the 3D separation since the fractional uncertainty of the latter two typically reach unity for sufficiently close pairs.

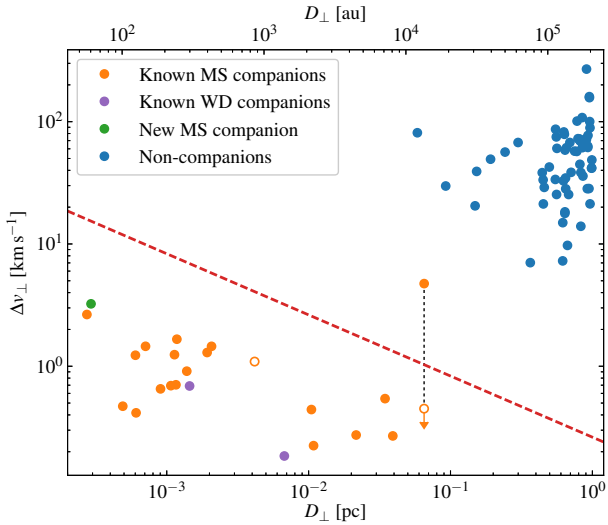


Figure 7. Tangential velocity differences as a function of projected separation for all *Gaia* sources within 1 pc of the white dwarfs in our 20 pc sample. The *Gaia* uncertainties in both D_{\perp} and Δv_{\perp} are smaller than the size of the points. For WD 0743–336/171 Pup A, the nominal *Gaia* value of Δv_{\perp} is shown by the solid point, which is joined to the corrected upper limit calculated from PPMXL data. The hollow point at $D_{\perp} = 859$ au corresponds to WD 2057–493/WISEA J210104.88–490626.5, which is not directly recovered by our search due to inaccuracy of the companion parallax. The red dashed line indicates the maximum Δv_{\perp} for a binary system containing two $1 M_{\odot}$ stars on circular orbits with a semimajor-axis of $D_{\perp}/2$.

(Table 5), we interpret the correlation to result from the relative orbital motion between binary components. The red dashed line in Fig. 7 indicates the maximum allowable Δv_{\perp} for a pair of $1 M_{\odot}$ stars separated by D_{\perp} , and on circular orbits, which is a power-law of $\Delta v_{\perp} \propto D_{\perp}^{-1/2}$. This runs approximately parallel to the top of the binary distribution (in log-log space), indicating that, for systems in the Solar neighbourhood, *Gaia* astrometry is indeed sensitive to wide binary orbital motions.

A clear outlier within Fig. 7 is WD 0743–033 and its established companion 171 Pup A, which are separated by $\approx 13\,400$ au and with $\Delta v_{\perp} \approx 4.7$ km s $^{-1}$. At face-value, this velocity difference and projected separation implies the two objects are gravitationally unbound. However, 171 Pup A suffers astrometric excess noise of 1.7 mas, which we attribute to its unresolved companion (Tokovinin et al. 2012). We checked the PPMXL proper motion (Roeser et al. 2010) for 171 Pup A, finding $(\mu_{\text{Ra}}, \mu_{\text{Dec}}) = (-276.8 \pm 2.3, 1679.3 \pm 2.4)$ mas yr $^{-1}$. Both PPMXL components are significantly different from the *Gaia* values, but within 1σ of the *Gaia* proper motion for WD 0743–336 (Table 5). Given the precision of the PPMXL proper motion, we determined an upper-limit to Δv_{\perp} of 0.45 km s $^{-1}$ (95 percent confidence), shown by the hollow point joined to the *Gaia* value in Fig. 7.

For similar reasons, the known companion to WD 2057–493 (WISEA J210104.88–490626.5, Kirkpatrick et al. 2016) failed to pass our initial selection criteria due to astrometric excess noise. The white dwarf has a *Gaia* par-

allax of 74.89 ± 0.04 mas, whereas 65.65 ± 0.49 mas is found for the companion, but with an `ASTROMETRIC_EXCESS_NOISE` of 2.3 mas. Therefore, the fairly liberal cut given by Equation (8) still causes this system to be missed. Unlike for WD 0743–033/171 Pup A, the proper motions for this pair are comparable. Adopting the parallax of the white dwarf, D_{\perp} and Δv_{\perp} are respectively inferred to be 858.54 ± 0.46 au and 1.091 ± 0.086 km s $^{-1}$, indicated by the hollow point in Fig. 7. The astrometric excess noise potentially indicates that WISEA J210104.88–490626.5 is itself an unresolved binary (similarly to 171 Pup A), in which case the system would be a hierarchical triple.

Overall, we found our methodology to be successful in identifying wide binary systems for local *Gaia* stars. With the exceptions of WD 0743–033 and WD 2057–493 described above, all other 20 pc white dwarfs with known companions that ought to be re-detected, were easily re-identified in Fig. 7. We note that the known companions to WD 0642–166 (Sirius B), WD 1009–184, and WD 2341+322 are not present in DR2 with five-parameter astrometry, and ostensibly were not recovered in our search. Similarly, five known white dwarfs in wide binaries, WD 0208–510, WD 0413–077, WD 0727+482A/B, and WD 0736+053 (Table 4) are themselves absent from DR2 (with the exception of Procyon, their companions *are* present), and so are also not recovered. We also acknowledge that our methodology is not free of limitations. The described method runs in $O(N^2)$ -time for N stars, of which some fraction are white dwarfs. Thus, in terms of search radius, r , the search time scales as $O(r^6)$. Furthermore, astrometric excess noise can prohibit the identification of some pairs if the astrometry for either component are strongly affected. This is problematic for identifying hierarchical multiples where one component is an unresolved binary, as was found already for WD 0743–033/171 Pup. One final limitation is that our method depends on the high astrometric precision found predominantly for local white dwarfs. In Table 5 we typically measured Δv_{\perp} to a precision of a few 0.01 km s $^{-1}$. Beyond 100 pc where many white dwarfs have $G \sim 20$, an uncertainty of a several km s $^{-1}$ can be expected instead. In such cases, the standard approach of proper motion comparison would prove more appropriate.

In summary we have identified 23 wide pairs containing white dwarfs within the *Gaia* DR2 data. Of these 23, 21 are wide white dwarf plus main-sequence star (WD+MS) binaries with two containing newly identified white dwarfs. Two of these WD+MS systems were not directly recovered by our method because of high astrometric excess noise of the companions, although are included in Fig. 7 and Table 5 for completeness. For six previously known WD+MS binaries, either the white dwarf or the main-sequence star is missing from *Gaia* DR2. Additionally, we recovered two known spatially resolved white dwarf plus white dwarf (WD+WD) binaries while one known system is missing from *Gaia* DR2. The binary population synthesis from Toonen et al. (2017) predicts numbers of resolved WD+MS and WD+WD systems that are in the range 23–43 and 16–30, respectively. We note that these ranges have been updated to account for the higher spatial resolution of *Gaia* than that of the ground-based observations assumed in Toonen et al. (2017). These numbers can decrease by 15–30 percent if we consider the possible disruption of weakly bound binaries by Galactic interactions. The lack of wide WD+WD binaries compared

to the population model found by [Toonen et al. \(2017\)](#) based on the ground-based 20 pc sample is confirmed with the significantly improved quality of the *Gaia* observations.

4.2 Unresolved double degenerate candidates

The *Gaia* sample includes one confirmed close double degenerate, WD 0135–052 ([Toonen et al. 2017](#)) and six white dwarfs, WD 0121–429, WD 0233–242, WD 0503–174, WD 0839–327, WD 2048+263, and WD 2248+293, previously described as double degenerate candidates in [Giammichele et al. \(2012\)](#). *Gaia* does not resolve any of these objects, and in all but two cases our *Gaia* atmospheric parameters (Table 1) using a single star model suggest a very low surface gravity inconsistent with single star evolution. The two exceptions are WD 0503–174 and WD 0839–327 which are in the low surface gravity tail of our distribution in Fig. 4 but do not stand out as particular outliers. Therefore, *Gaia* data alone is insufficient to confirm the nature of these two objects and spectroscopy is needed for a full diagnostic. From our *Gaia* atmospheric parameters we do not identify any new double degenerate candidates, especially when considering the trend of systematically lower surface gravities at cool T_{eff} in Fig. 4. Of the new systems, we found that *Gaia* DR2 2486388560866377856 has a $\log g = 7.67$ from our atmospheric fit. However, the star appears only 4 arcsec away from its much brighter companion, and thus its photometry may have been contaminated.

The updated models (accounting for the enhanced resolution of *Gaia*) of [Toonen et al. \(2017\)](#) upredict 0.5–7.0 unresolved double white dwarfs within 20 pc and therefore the population synthesis model remains in agreement with the observations.

4.3 Unresolved main-sequence + white dwarf binaries

We do not identify any unresolved white dwarf plus main-sequence binaries in the 20 pc *Gaia* sample. The two previously known systems, WD 0419–487 and WD 0454+620 ([Toonen et al. 2017](#)) are confirmed (Table 2) or suspected (Table 4) to be beyond 20 pc, respectively. Since [Toonen et al. \(2017\)](#), we became aware of two very likely unresolved white dwarf plus main-sequence binaries:

G 203–47ab was identified by [Reid & Gizis \(1997\)](#) as a single-lined binary with a M3.5 dwarf primary, and [Delfosse et al. \(1999\)](#) determined an orbital period of 14.7136 ± 0.005 d and a low eccentricity, $e = 0.068 \pm 0.004$. Adopting a mass of $0.2 M_{\odot}$ for the M3.5 primary, [Delfosse et al. \(1999\)](#) derived a lower limit on the mass of the companion of $0.5 M_{\odot}$, implying that it has to be a degenerate stellar remnant. Based on the detected $U - B$ colour excess of G203–47ab, [Delfosse et al. \(1999\)](#) argue that it is most likely a white dwarf. The close proximity of this system, $D = 7.43 \pm 0.03$ pc, affects the claimed completeness of the 13 pc sample. The white dwarf nature could possibly be confirmed with ultraviolet observations (G203–47ab is detected in the *GALEX* survey with $FUV = 21.85$ mag and $NUV = 19.58$ mag). This system is found in DR2 with a source ID 1355264565043431040 and parallax 134.60 ± 0.49 mas.

Wolf 1130AB is a single-lined binary with an orbital

period of 0.4967 d, found by [Mace et al. \(2018\)](#) at a distance of 16.7 ± 0.2 pc. The primary star is an M-subdwarf with a mass of $\approx 0.3 M_{\odot}$, which is tidally locked, as established from the photometric V -band modulation. The *Gaia* DR1 parallax and projected rotational velocity were combined to tightly constrain the inclination, and hence the mass of the unseen companion, Wolf 1130B, to $1.24^{+0.19}_{-0.15} M_{\odot}$. The DR2 parallax of this system is 60.391 ± 0.034 mas ($D = 16.550 \pm 0.009$ pc) with DR2 source ID 2185716209919937664.

Just as ground-based observations, *Gaia* is unable to detect faint white dwarfs outshone by bright companions in the optical hence our sample may be incomplete in this respect. Using different theoretical assumptions regarding binary evolution and Galactic stellar formation history, [Toonen et al. \(2017\)](#) predict 0.5–1.6 unresolved white dwarf plus main sequence binaries within 20 pc at the enhanced resolution of *Gaia*. While *Gaia* DR2 can not easily detect new binaries of these types, the small predicted number suggests it does not significantly impact the estimation of the white dwarf space-density. Binaries sufficiently wide to produce an astrometric perturbation, such as suspected for G 203–47ab ([Delfosse et al. 1999](#)), may be identified by future *Gaia* data releases.

5 SPACE-DENSITY

Despite the precision of *Gaia* parallaxes and the new white dwarf identifications, estimating the white dwarf space-density from our *Gaia* DR2 sample is not trivial. Of the known degenerate stars, some of those within (or thought to be within) 20 pc do not have *Gaia* 5-parameter astrometric solutions. This primarily affects the closest systems with large proper motions, but also a few objects between 10 and 20 pc. To accurately calculate the local white dwarf space-density it is thus important to consider the incompleteness of this sample, and how this varies as a function of distance.

We assumed that the *Gaia* 20 pc white dwarfs are drawn from a selection function, $S(\vec{\theta}, D)$, representing the probability of detection as a function of distance,⁷ D , and where $\vec{\theta}$ is the parameter vector defining S (whose shape we would like to estimate). With a prescription of S , we then simply look at how previously known white dwarfs are re-detected in *Gaia* DR2 as a function of distance. To constrain S , we chose the sample of white dwarfs which were previously estimated to be within 3σ of 20 pc, and where a parallax was available before DR2. We enforced the requirement of prior parallaxes because many of the white dwarfs with only spectroscopic distances turned out to be predominantly much farther away than expected upon release of DR2 data (Table 2). Furthermore, objects where previous parallaxes suggested potential 20 pc membership, but are now known to be beyond 20 pc were still included – their exclusion would bias the sample towards non-detections near 20 pc, and their inclusion only acts to further constrain S slightly beyond 20 pc. For the re-detected objects we used the updated distances from their new *Gaia* parallaxes. One final point of note, is that we counted both members of wide double degenerates as a single detection, since their *Gaia* detection/non-detection are not independent.

⁷ While this selection function can be explored in terms of proper

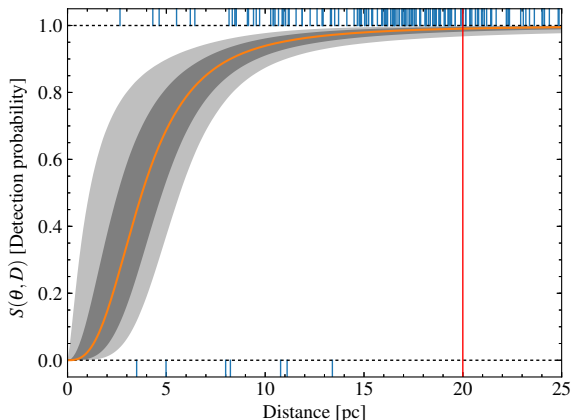


Figure 8. Our fit to the selection function, $S(\vec{\theta}, D)$. The grey regions represent the 1 and 2 σ contours on the fit, with the median given in orange. The blue lines indicate the locations of detections vs. non-detections for known white dwarfs within 20 pc (to within 3 σ) prior to DR2.

As re-detection is a binary-categorical variable, estimation of $\vec{\theta}$ is naturally suited to logistic regression. We define S in terms of the logistic function,⁸

$$S(\vec{\theta}, D) = \frac{1}{1 + \exp(-f(\vec{\theta}, D))}, \quad (10)$$

where we define $f(\vec{\theta}, D) = \theta_0 \log(D/\text{pc}) + \theta_1$, i.e. a first order polynomial in the natural logarithm of D .

Regardless of the detailed formulation of Equation (10), the likelihood of a re-detection for a single white dwarf is a Bernoulli trial with probability S . For a set of detections and non-detections, their combined likelihood is therefore given by

$$L = P(\vec{y}|\vec{\theta}, \vec{D}) = \prod_i^N S_i^{y_i} (1 - S_i)^{1-y_i}, \quad (11)$$

where $y_i = 1$ for a detection, $y_i = 0$ for a non-detection, and $S_i = S(\vec{\theta}, D_i)$.

To estimate the values of $\vec{\theta}$ and their uncertainties, we used the MCMC ensemble sampler EMCEE (Foreman-Mackey et al. 2013) to sample the log-likelihood,⁹ which can be simplified to

$$\log L = \sum_{y_i=1} \log(S_i) + \sum_{y_i=0} \log(1 - S_i). \quad (12)$$

From the results of our MCMC, we found θ_0 and θ_1 were 2.83 ± 0.80 and -3.7 ± 1.8 respectively, with a correlation of

motion, magnitude, or sky-position, etc., for a space-density estimate we are required to work with distances.

⁸ With this formulation of S , $f(\vec{\theta}, D)$ is equivalent to the log-odds-ratio, mapping \mathbb{R} to the interval $[0, 1]$.

⁹ From a Bayesian perspective, our intention is ultimately to estimate $P(\vec{\theta}|D_i, y_i)$, the posterior distribution on $\vec{\theta}$. Lacking any informed priors on $\vec{\theta}$, our sampling of the log-likelihood, is equivalent to assuming improper uniform priors on both $\vec{\theta}$ components.

-0.969 between the two. The corresponding selection function is shown in Fig. 8 (orange), with its 1 σ and 2 σ error-contours in grey. This is clearly much better constrained towards higher distances, due to the increased number of stars per unit distance. At the distance of Sirius B this corresponds to a detection probability of 28^{+24}_{-17} percent, but at 20 pc, this reaches $99.1^{+0.5}_{-1.0}$ percent. Integrating over S out to 20 pc, we determined the effective volume probed by *Gaia* given by

$$V_{\text{eff}} = 4\pi \int_0^{20} S(\vec{\theta}, D) D^2 dD. \quad (13)$$

Using the MCMC samples for $\vec{\theta}$ gave $V_{\text{eff}} = 32170^{+420}_{-540} \text{pc}^3$ implying a volume-averaged detection-efficiency of $96.0^{+1.3}_{-1.6}$ percent out to 20 pc for *Gaia* white dwarfs.

We calculated the local white dwarf space-density by propagating the uncertainties in all relevant quantities via a Monte-Carlo approach. While our DR2 sample contains 139 sources (Table 1), two systems have parallaxes that could allow them to reside either side of the 20 pc boundary. We found probabilities of $\approx 2/46/52$ percent for 137/138/139 systems within 20 pc respectively, which we used for our Monte-Carlo draws. Additionally WD 0135–052 is known to be an unresolved double degenerate system, therefore we added one to the above quantity to obtain the total white dwarf count, N_{Gaia} .

Accurately ascertaining the space-density required that we also constrain the number of missing white dwarfs (N_{missing}) within 20 pc. Using our Monte-Carlo samples for both N_{Gaia} and our estimate of the completeness (as calculated above) we determined N_{missing} using the negative-binomial distribution, which we found had a mode of five. However, eight white dwarfs that are confirmed 20 pc members are missing from our 20 pc sample (Table 4), providing a prior on the number of missing systems. Thus, we discarded all samples with values less than eight, with the remaining samples used for our estimate of N_{missing} . Our calculation for the total number of 20 pc white dwarfs is therefore given by $N_{\text{tot}} = N_{\text{Gaia}} + N_{\text{missing}}$. As a brief aside, $N_{\text{missing}} - 8$ estimates the remaining number of 20 pc white dwarfs that are yet to be discovered (Fig. 9), which has a mode of zero at 28 percent probability, a median of two, and a 95 percent upper limit of seven. Correspondingly the completeness for *all* white dwarfs within 20 pc (not just those in *Gaia*) has a median value of 98.7 percent, with 95.5 percent as a lower-limit (95 percent confidence). Therefore, there is a reasonable chance that all 20 pc white dwarfs have now been identified, though the prospect of several more members remains for future *Gaia* data releases.

We considered N_{tot} as drawn from a Poisson-process with mean \bar{N} . To correctly account for the Poisson-uncertainty associated with N_{tot} , we drew samples from a Gamma-distribution (the conjugate prior of the Poisson distribution) with a Jeffreys prior¹⁰ to constrain \bar{N} , finding $\bar{N} = 150.3 \pm 12.6$. Finally, by dividing by the volume of the entire 20 pc sphere, we arrived at our adopted space-density, $\rho = (4.49 \pm 0.38) \times 10^{-3} \text{pc}^{-3}$. In Fig. 10 we show the cumulative distribution for our *Gaia* sample compared with the expectation value from our space-density calculation.

While slightly lower than some other recent values, our adopted space-density is within 1 σ of these other estimates calculated from the local sample – $(4.8 \pm 0.5) \times 10^{-3} \text{pc}^{-3}$ was

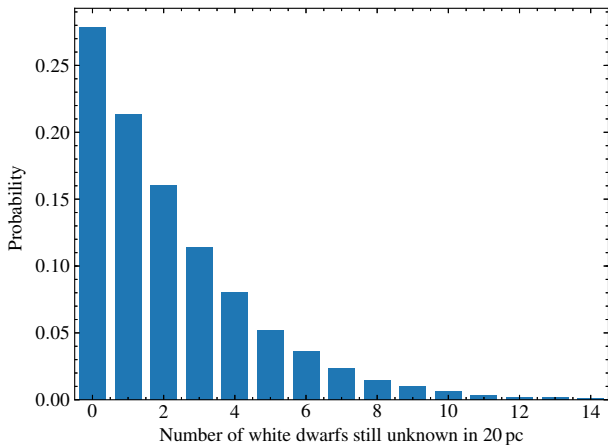


Figure 9. Probability distribution for the number of 20 pc white dwarfs that remain undetected both in *Gaia* and elsewhere.

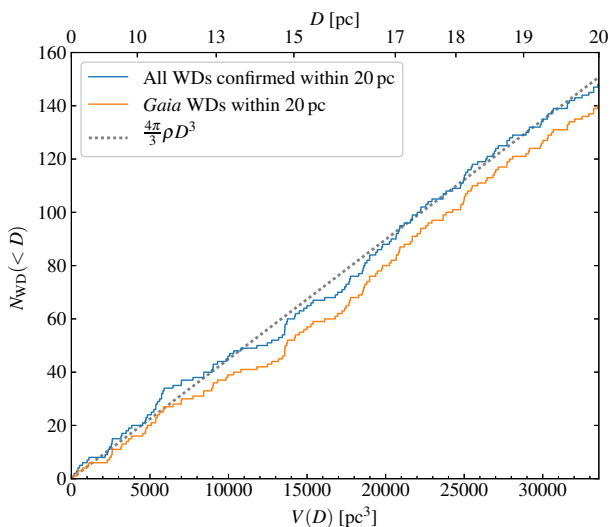


Figure 10. Cumulative number of all-known and *Gaia* white dwarfs as a function of enclosed volume (blue and orange respectively). The grey dotted line shows the expectation value at each distance for the adopted space-density. Note that the slope of this line depends only on the total number of objects enclosed within 20 pc, and does not represent a fit to the cumulative distribution. Fitting directly to the cumulative distribution is erroneous as the steps are not statistically independent, and leads to an underestimated uncertainty in the space-density.

reported by Holberg et al. (2016), $4.39 \times 10^{-3} \text{ pc}^{-3}$ by Giammichele et al. (2012), and $(4.9 \pm 0.5) \times 10^{-3} \text{ pc}^{-3}$ by Sion et al. (2009). Such close agreement should not come as a surprise as these samples necessarily contain some overlap, and are thus not statistically independent measurements. On the other hand, Munn et al. (2017) made an independent measurement of the space-density using ≈ 3000 SDSS white dwarfs finding $\rho = 5.5 \pm 0.1 \text{ pc}^{-3}$. While this value is in disagreement with our estimate at the 2.6σ level, we note that the uncertainty in the density adopted by Munn et al.

(2017) appears to be entirely statistical and does not, for instance, include possible uncertainty in the Galactic model used in their calculation. A fractional systematic uncertainty of 10 percent would be sufficient to resolve this discrepancy.

Further improvement to the precision of the local space-density will necessitate a vast increase in the number of objects, and thus an extension of this work to a larger volume. We do note however that our estimate for ρ does not consider white dwarfs hidden as close companions to bright main-sequence stars.

6 SUMMARY

We have revisited the 20 pc white dwarf local sample making use of the recently released *Gaia* DR2 data. The updated sample is now potentially complete for resolved sources, even for the most intrinsically faint white dwarfs. Within 20 pc, we identified 130 known white dwarfs, while having confirmed 57 candidate 20 pc members (but known white dwarfs) to be located at farther distances. From our Hertzsprung-Russell diagram, we identified 15 new 20 pc white dwarf candidates. Fitting not only the *Gaia* data, but also, where available, Pan-STARRS and 2MASS photometry, we established 9 of these to be newly identified white dwarfs (with the closest system found at 13.05 pc), with the remainder as likely main-sequence objects with adversely affected *Gaia* photometry/astrometry. Despite the high quality of the *Gaia* observations of very nearby stars, we therefore stress significant care has to be taken in the sample selection and data analysis to avoid misinterpreting the relatively large fraction of spurious sources. Spectroscopic follow-up observations of the newly identified white dwarfs and white dwarf candidates are encouraged to determine their photospheric properties. The rich diversity of spectral types and binary evolution paths observed in the currently characterised local sample (Giammichele et al. 2012; Toonen et al. 2017) means that it is a benchmark to understand stellar and binary evolution as well as the spectral evolution of the atmosphere of white dwarfs owing to carbon dredge-up, convective mixing, and the accretion of planetesimals (Dufour et al. 2005; Tremblay & Bergeron 2008; Gentile Fusillo et al. 2017; Hollands et al. 2018).

Making full use of the exquisite *Gaia* astrometry, we searched for wide companions to the white dwarfs in the 20 pc sample. For each white dwarf in the sample, we considered all stars within 1 pc, and compared tangential velocity differences with the projected separation to distinguish companions. Of the known wide binaries containing white dwarfs where both components were found in DR2, all but two were easily re-identified (17 WD+MS and 2 WD+WD binaries). The companions to the other two white dwarfs either had an inaccurate proper motion or parallax owing to their high astrometric excess noise. Of the nine new white dwarfs, we found one of these has a wide M dwarf companion. We did not identify any companions to known white dwarfs that were hitherto undiscovered. Since no new resolved WD+WD systems were identified, the total number of wide double degenerate systems within 20 pc of the Sun remains at three,

¹⁰ The Jeffreys prior for the rate parameter, λ , of the Poisson distribution is $P(\lambda) \propto \lambda^{-1/2} \equiv \text{Gamma}(1/2, 0)$.

including one pair absent from the *Gaia* astrometry. This observational finding remains in contrast with the most recent binary population synthesis models which instead predict 16–30 such systems. In terms of unresolved binaries, we did not identify any new systems. Candidate systems identified elsewhere remain as such, with none being partially resolved into two components. High-resolution, time-resolved spectroscopic follow-up will be required to confirm their binarity one way or the other. In any case, the number of confirmed unresolved binaries (both WD+WD and WD+MS systems) remain consistent with the expected values from binary population models.

With this up-to-date sample in hand we calculated a new estimate of the local white dwarf space density. To be as accurate as possible in this calculation, we placed statistical constraints on the number of white dwarfs remaining undetected within 20 pc. For this purpose, we first assessed the re-detection rate of known white dwarfs as a function of distance, and found that while *Gaia* does not reliably detect white dwarfs at the very closest distances, the detection probability is close to 100 percent at 20 pc. This implied that white dwarfs are found by *Gaia* with an overall detection efficiency of $96.0^{+1.3}_{-1.6}$ percent within the 20 pc volume. Considering 8 degenerate stars that did not have *Gaia* DR2 and that have been firmly established elsewhere as 20 pc members, we found an upper limit of 7 for the number of 20 pc white dwarfs remaining to be found. Folding this uncertainty into our calculations, we determined the local white dwarf space density to be $(4.49 \pm 0.38) \times 10^{-3} \text{ pc}^{-3}$, which we found to be consistent with, but more precise than previous values determined from local white dwarfs. Because we find the 20 pc sample is now close to complete, more precise estimates of the local white dwarf space-density will necessitate extending this work to larger volume-complete samples.

While we have successfully assessed many properties of the local *Gaia* white dwarf population, this represents only a subset of white dwarf related science that can be probed with *Gaia*. For example, the statistics of local white dwarfs with magnetic fields or metal-pollution were considered beyond the scope of this work, but represent potential avenues of future investigation using *Gaia* data. More generally, magnitude-limited *Gaia* white dwarf samples will naturally contain several orders of magnitude more stars than any local sample, but at the expense of increased selection bias. We therefore expect this work to be useful as a comparison sample in these cases. Future *Gaia* data releases will allow the extension of the volume-complete local sample to greater distances as an increased number of faint objects acquire full 5-parameter astrometry.

ACKNOWLEDGEMENTS

The research leading to these results has received funding from the European Research Council under the European Union's Seventh Framework Programme (FP/2007- 2013) / ERC Grant Agreement n. 320964 (WDTracer) and under the European Union's Horizon 2020 research and innovation programme n. 677706 (WD3D).

REFERENCES

- Bailer-Jones C. A. L., 2015, *PASP*, **127**, 994
- Bailer-Jones C. A. L., Rybizki J., Foesneau M., Man-telet G., Andrae R., 2018, preprint, [p. arXiv:1804.10121](https://arxiv.org/abs/1804.10121) ([arXiv:1804.10121](https://arxiv.org/abs/1804.10121))
- Bergeron P., et al., 2011, *ApJ*, **737**, 28
- Blouin S., Kowalski P. M., Dufour P., 2017, *ApJ*, **848**, 36
- Borysov A., Jorgensen U. G., Fu Y., 2001, *J. Quant. Spectrosc. Radiat. Transfer*, **68**, 235
- Buckner A. S. M., Froebrich D., 2014, *MNRAS*, **444**, 290
- Caballero J. A., 2010, *A&A*, **514**
- Chambers K. C., et al., 2016, preprint, ([arXiv:1612.05560](https://arxiv.org/abs/1612.05560))
- Chiba M., Beers T. C., 2000, *AJ*, **119**, 2843
- Cohen M., Wheaton W. A., Megeath S. T., 2003, *AJ*, **126**, 1090
- Delfosse X., Forveille T., Mayor M., Burnet M., Perrier C., 1999, *A&A*, **341**, L63
- Dittmann J. A., et al., 2017, *Nat*, **544**, 333
- Duchêne G., Kraus A., 2013, *Annual Review of Astronomy and Astrophysics*, **51**, 269
- Dufour P., Bergeron P., Fontaine G., 2005, *ApJ*, **627**, 404
- Duquenois A., Mayor M., 1991, *A&A*, **248**, 485
- El-Badry K., Rix H.-W., Weisz D. R., 2018, *ApJ*, **860**, L17
- Evans D. W., et al., 2018, preprint, ([arXiv:1804.09368](https://arxiv.org/abs/1804.09368))
- Farihi J., Burleigh M. R., Holberg J. B., Casewell S. L., Barstow M. A., 2011, *MNRAS*, **417**, 1735
- Ferrario L., 2012, *MNRAS*, **426**, 2500
- Finch C. T., Zacharias N., 2016, *AJ*, **151**, 160
- Finch C. T., Zacharias N., Subasavage J. P., Henry T. J., Riedel A. R., 2014, *AJ*, **148**, 119
- Finch C. T., Zacharias N., Jao W.-C., 2018, *AJ*, **155**, 176
- Fontaine G., Brassard P., Bergeron P., 2001, *PASP*, **113**, 409
- Foreman-Mackey D., Hogg D. W., Lang D., Goodman J., 2013, *PASP*, **125**, 306
- Fuchs B., Jahreiß H., 1998, *A&A*, **329**, 81
- Fuhrmann K., Chini R., Hoffmeister V. H., Bernkopf J., 2012, *MNRAS*, **420**, 1423
- Fuhrmann K., Chini R., Kaderhandt L., Chen Z., 2017a, *MNRAS*, **464**, 2610
- Fuhrmann K., Chini R., Kaderhandt L., Chen Z., Lachaume R., 2017b, *MNRAS*, **471**, 3768
- Fuhrmann K., Chini R., Kaderhandt L., Chen Z., 2017c, *ApJ*, **836**, 139
- Gaia Collaboration et al., 2018b, preprint, ([arXiv:1804.09378](https://arxiv.org/abs/1804.09378))
- Gaia Collaboration Brown A. G. A., Vallenari A., Prusti T., de Bruijne J. H. J., Babusiaux C., Bailer-Jones C. A. L., 2018a, preprint, ([arXiv:1804.09365](https://arxiv.org/abs/1804.09365))
- Garcia-Berro E., Ritossa C., Iben I. J., 1997, *ApJ*, **485**, 765
- Genest-Beaulieu C., Bergeron P., 2014, *ApJ*, **796**, 128
- Gentile Fusillo N. P., Gänsicke B. T., Farihi J., Koester D., Schreiber M. R., Pala A. F., 2017, *MNRAS*, **468**, 971
- Giannichele N., Bergeron P., Dufour P., 2012, *ApJS*, **199**, 29
- Gianninas A., Bergeron P., Ruiz M. T., 2011, *ApJ*, **743**, 138
- Gianninas A., Curd B., Thorstensen J. R., Kilic M., Bergeron P., Andrews J. J., Canton P., Agüeros M. A., 2015, *MNRAS*, **449**, 3966
- Girard T. M., et al., 2011, *AJ*, **142**, 15
- Gliese W., Jahreiß H., 1991, Technical report, Preliminary Version of the Third Catalogue of Nearby Stars
- Heintz W. D., 1993, *AJ*, **105**, 1188
- Henry T. J., et al., 2018, *AJ*, **155**, 265
- Holberg J. B., Oswalt T. D., Sion E. M., 2002, *ApJ*, **571**, 512
- Holberg J. B., Sion E. M., Oswalt T., McCook G. P., Foran S., Subasavage J. P., 2008, *AJ*, **135**, 1225
- Holberg J. B., Oswalt T. D., Sion E. M., Barstow M. A., Burleigh M. R., 2013, *MNRAS*, **435**, 2077
- Holberg J. B., Oswalt T. D., Sion E. M., McCook G. P., 2016, *MNRAS*, **462**, 2295

- Hollands M. A., Gänsicke B. T., Koester D., 2018, *MNRAS*, **477**, 93
- Iben I. J., Ritossa C., Garcia-Berro E., 1997, *ApJ*, **489**, 772
- Joshi Y. C., Dambis A. K., Pandey A. K., Joshi S., 2016, *A&A*, **593**, A116
- Kepler S. O., et al., 2016, *MNRAS*, **455**, 3413
- Kilic M., Hambly N. C., Bergeron P., Genest-Beaulieu C., Rowell N., 2018, *MNRAS*, p. L114
- Kirkpatrick J. D., et al., 2016, *ApJS*, **224**, 36
- Koester D., Gänsicke B. T., Farihi J., 2014, *A&A*, **566**, A34
- Kowalski P. M., Saumon D., 2006, *ApJ Lett.*, **651**, L137
- Lépine S., Thorstensen J. R., Shara M. M., Rich R. M., 2009, *AJ*, **137**, 4109
- Liebert J., Bergeron P., Holberg J. B., 2005, *ApJS*, **156**, 47
- Limoges M.-M., Bergeron P., Lépine S., 2015, *ApJS*, **219**, 19
- Lindgren L., et al., 2018, preprint, ([arXiv:1804.09366](https://arxiv.org/abs/1804.09366))
- Luyten W. J., 1997, VizieR Online Data Catalog, **1130**
- Luyten W. J., Hughes H. S., 1980, Proper Motion Survey, University of Minnesota, **55**
- Mace G. N., et al., 2018, *ApJ*, **854**, 145
- Massey P., Meyer M., 2001, *Stellar Masses*. Bristol: Institute of Physics Publishing, p. 1882, [doi:10.1888/0333750888/1882](https://doi.org/10.1888/0333750888/1882)
- Moe M., Di Stefano R., 2017, *The Astrophysical Journal Supplement Series*, **230**, 15
- Munn J. A., et al., 2017, *AJ*, **153**, 10
- Pesch P., Sanduleak N., 1978, *AJ*, **83**, 1090
- Platais I., et al., 1998, *AJ*, **116**, 2556
- Press W., Teukolsky S., Vetterling W., Flannery B., 1992, *Numerical Recipes in FORTRAN 77*. Cambridge Univ. Press, Cambridge
- Raghavan D., et al., 2010, *The Astrophysical Journal Supplement Series*, **190**, 1
- Rebassa-Mansergas A., Rybicka M., Liu X.-W., Han Z., García-Berro E., 2015, *MNRAS*, **452**, 1637
- Reid I. N., Gizis J. E., 1997, *AJ*, **113**, 2246
- Reylé C., Scholz R., Schultheis M., Robin A. C., Irwin M., 2006, *MNRAS*, **373**, 705
- Roeser S., Demleitner M., Schilbach E., 2010, *AJ*, **139**, 2440
- Sayres C., Subasavage J. P., Bergeron P., Dufour P., Davenport J. R. A., AlSayyad Y., Tofflemire B. M., 2012, *AJ*, **143**, 103
- Scholz R. D., Meusinger H., Jahreiß H., 2018, *A&A*, **613**, A26
- Sion E. M., Holberg J. B., Oswalt T. D., McCook G. P., Wasatonic R., 2009, *AJ*, **138**, 1681
- Sion E. M., Holberg J. B., Oswalt T. D., McCook G. P., Wasatonic R., Myszka J., 2014, *AJ*, **147**, 129
- Skrutskie M. F., et al., 2006, *AJ*, **131**, 1163
- Smartt S. J., Eldridge J. J., Crockett R. M., Maund J. R., 2009, *MNRAS*, **395**, 1409
- Smith L. C., et al., 2018, *MNRAS*, **474**, 1826
- Subasavage J. P., Henry T. J., Bergeron P., Dufour P., Hambly N. C., Beaulieu T. D., 2007, *AJ*, **134**, 252
- Subasavage J. P., Henry T. J., Bergeron P., Dufour P., Hambly N. C., 2008, *AJ*, **136**, 899
- Subasavage J. P., Jao W.-C., Henry T. J., Bergeron P., Dufour P., Ianna P. A., Costa E., Méndez R. A., 2009, *AJ*, **137**, 4547
- Subasavage J. P., et al., 2017, *AJ*, **154**, 32
- Tokovinin A., 2014, *AJ*, **147**, 86
- Tokovinin A., Hartung M., Hayward T. L., Makarov V. V., 2012, *AJ*, **144**
- Tonry J. L., et al., 2012, *ApJ*, **750**, 99
- Toonen S., Hollands M., Gänsicke B. T., Boekholt T., 2017, *A&A*, **602**, A16
- Tremblay P.-E., Bergeron P., 2008, *ApJ*, **672**, 1144
- Tremblay P.-E., Ludwig H.-G., Steffen M., Bergeron P., Freytag B., 2011, *A&A*, **531**, L19+
- Tremblay P.-E., Ludwig H.-G., Steffen M., Freytag B., 2013, *A&A*, **559**, A104
- Tremblay P.-E., Leggett S. K., Lodieu N., Freytag B., Bergeron P., Kalirai J. S., Ludwig H.-G., 2014a, *ApJ*, **788**, 103
- Tremblay P.-E., Kalirai J. S., Soderblom D. R., Cignoni M., Cummings J., 2014b, *ApJ*, **791**, 92
- Tremblay P.-E., Cummings J., Kalirai J. S., Gänsicke B. T., Gentile-Fusillo N., Raddi R., 2016, *MNRAS*, **461**, 2100
- Tremblay P.-E., et al., 2017, *MNRAS*, **465**, 2849
- Wegg C., Phinney E. S., 2012, *MNRAS*, **426**, 427
- Winget D. E., Hansen C. J., Liebert J., van Horn H. M., Fontaine G., Nather R. E., Kepler S. O., Lamb D. Q., 1987, *ApJ Lett.*, **315**, L77
- Zacharias N., Monet D. G., Levine S. E., Urban S. E., Gaume R., Wycoff G. L., 2004, in *American Astronomical Society Meeting Abstracts*. p. 48.15
- van Altena W. F., Lee J. T., Hoffleit E. D., 1995, *The general catalogue of trigonometric [stellar] parallaxes*
- van Leeuwen F., 2007, *A&A*, **474**, 653

Table 1: Astrometric and photometric data for our *Gaia* 20 pc white dwarf sample, as well as the results from our model atmosphere fits from Section 2.1. The column comp. refers to the adopted atmospheric composition used for our fits to the *Gaia* photometry and parallaxes. Note that the coordinates are given in the *Gaia* DR2 J2015.5 epoch, and so must be corrected by the proper motions for direct comparison with the J2000 epoch. The parallaxes are given without the 0.03 mas offset suggested by Lindegren et al. (2018).

J2015.5	WD	<i>Gaia</i> DR2 ID	ϖ [mas]	μ_{α} [mas yr ⁻¹]	μ_{δ} [mas yr ⁻¹]	<i>G</i> [mag]	<i>G</i> _{BP} [mag]	<i>G</i> _{RP} [mag]	spType	comp.	T_{eff} [K]	log <i>g</i> [dex]	Note
000211.59-43.1006.0	2359-434	499487709497259264	119.98 ± 0.03	+613.64 ± 0.04	-686.73 ± 0.04	12.9137 ± 0.0004	12.9943 ± 0.0034	12.7015 ± 0.0009	DAC	H	8464 ± 21	8.36 ± 0.01	
000240.29-34.1351.4	0000-345	2312821266302222720	67.54 ± 0.04	+152.20 ± 0.06	-762.18 ± 0.06	14.8943 ± 0.0005	15.1187 ± 0.0040	14.4948 ± 0.0020	DAP	He	6327 ± 29	8.14 ± 0.01	
000720.92+10.2017.6	0004+122	27662344439302571904	57.31 ± 0.11	+354.94 ± 0.18	-232.26 ± 0.11	16.2650 ± 0.0008	16.6828 ± 0.0062	15.6775 ± 0.0032	DC	He	5116 ± 24	8.21 ± 0.02	
001214.00+5.20512.2	0009+501	395234439752169344	91.98 ± 0.03	+461.37 ± 0.04	-551.63 ± 0.02	14.2474 ± 0.0002	14.4704 ± 0.0020	13.8494 ± 0.0009	DAH	H	6476 ± 11	8.24 ± 0.01	
001350.66-71.4958.1	0011-721	4689789625044431616	53.23 ± 0.03	-263.03 ± 0.04	-247.70 ± 0.04	15.0466 ± 0.0005	15.2958 ± 0.0025	14.6254 ± 0.0017	DA	H	6271 ± 18	7.87 ± 0.01	
001412.21-13.1112.2	0011-134	2418116963320446720	53.81 ± 0.07	-546.70 ± 0.10	-714.86 ± 0.08	15.7657 ± 0.0006	16.0738 ± 0.0035	15.2799 ± 0.0027	DAH	H	5858 ± 22	8.20 ± 0.01	
004125.51-2221.08.2	0038-226	2349916559152267008	109.88 ± 0.03	-463.23 ± 0.04	-381.77 ± 0.03	14.3074 ± 0.0002	14.6778 ± 0.0013	13.7647 ± 0.0010	DQpec	H+He	5162 ± 12	7.86 ± 0.01	1
004911.18+05.2237.0	0046+051	2552928187080872832	231.74 ± 0.04	+1231.33 ± 0.08	-2711.83 ± 0.04	12.3122 ± 0.0001	12.5531 ± 0.0006	11.9427 ± 0.0005	DZ	He	6424 ± 5	8.25 ± 0.01	
011800.06+16.1010.5	0115+159	2591754107321120896	59.61 ± 0.04	-17.15 ± 0.07	-650.57 ± 0.07	13.8031 ± 0.0005	13.8261 ± 0.0043	13.6846 ± 0.0017	DQ	He	9755 ± 48	8.23 ± 0.01	
012404.41-42.4046.6	0121-429	4983839647522981504	54.12 ± 0.02	-238.19 ± 0.03	-524.33 ± 0.03	14.7051 ± 0.0003	14.9778 ± 0.0015	14.2568 ± 0.0011	DAH	H	6068 ± 10	7.57 ± 0.01	
012524.74-26.0005.6	0123-242	503708487246444928	60.40 ± 0.02	-295.91 ± 0.08	-524.51 ± 0.05	14.9729 ± 0.0003	15.1162 ± 0.0025	14.6687 ± 0.0011	DC	He	7212 ± 18	8.35 ± 0.01	
013800.00-04.5950.1	0135-052	2480523216087975040	79.21 ± 0.04	+580.95 ± 0.07	-350.18 ± 0.06	12.7584 ± 0.0003	12.9246 ± 0.0022	12.4416 ± 0.0009	DA	H	7190 ± 15	7.25 ± 0.01	
014300.10-67.1846.1	0141-675	4698424845771339520	102.90 ± 0.01	-329.28 ± 0.03	-1018.46 ± 0.02	13.7087 ± 0.0003	13.9498 ± 0.0021	13.2995 ± 0.0014	DAZ	H	6359 ± 15	7.98 ± 0.01	
015151.68+64.2549.4	0148+641	518201792978858880	57.77 ± 0.02	+224.82 ± 0.03	-201.52 ± 0.03	13.9649 ± 0.0002	14.0352 ± 0.0023	13.7789 ± 0.0013	DA	H	8796 ± 28	8.10 ± 0.01	
015202.97+47.0008.5	0148+467	356922880493142016	60.39 ± 0.07	+4.91 ± 0.09	+121.77 ± 0.11	12.5156 ± 0.0004	12.4589 ± 0.0031	12.5937 ± 0.0019	DA	H	14340 ± 117	8.00 ± 0.01	
021122.23+39.9551.3	0208+396	333010327952701696	58.23 ± 0.04	+1028.73 ± 0.07	-500.37 ± 0.06	14.4213 ± 0.0004	14.5789 ± 0.0033	14.1038 ± 0.0014	DAZ	H	7196 ± 22	7.94 ± 0.01	
021228.34-08.0417.9		2486388560866377856	59.88 ± 0.05	-609.29 ± 0.10	-448.00 ± 0.08	13.7376 ± 0.0006	13.7996 ± 0.0078	13.4503 ± 0.0044					2, 3
021349.04-33.4524.4		4970215770740383166	53.23 ± 0.11	+172.64 ± 0.13	+361.30 ± 0.15	15.9736 ± 0.0014	15.9551 ± 0.0284	15.1438 ± 0.0185					
022327.94-14.4120.3	0230-144	5146358420863612160	59.99 ± 0.06	+307.59 ± 0.08	-681.78 ± 0.09	15.5914 ± 0.0008	15.9882 ± 0.0055	15.0339 ± 0.0025	DA	H	5388 ± 21	7.98 ± 0.02	
023521.67-24.0005.6	0233-242	512518629678747008	54.07 ± 0.05	-105.93 ± 0.08	-607.11 ± 0.07	15.6863 ± 0.0007	16.1807 ± 0.0058	15.0248 ± 0.0038	DC	H	4842 ± 25	7.50 ± 0.02	
024835.68+5.42316.5	0245+541	453562088496088320	92.03 ± 0.04	+423.45 ± 0.08	-385.24 ± 0.07	15.1302 ± 0.0004	15.6184 ± 0.0025	14.4885 ± 0.0016	DAZ	H	4928 ± 11	8.00 ± 0.01	
031031.13-68.3605.0	0310-688	4646535078125821568	96.17 ± 0.04	+39.45 ± 0.10	-103.19 ± 0.09	11.4198 ± 0.0005	11.3452 ± 0.0008	11.5373 ± 0.0012	DA	H	16407 ± 116	8.11 ± 0.01	
032151.29-01.4928.5	0322-019	3261591090771914240	59.12 ± 0.12	+236.02 ± 0.13	-868.88 ± 0.13	15.9166 ± 0.0012	16.3534 ± 0.0048	15.3225 ± 0.0043	DAZH	H	5173 ± 27	8.06 ± 0.02	
034435.30+18.2552.3	0341+182	44901791432527232	53.00 ± 0.05	+142.68 ± 0.10	-1129.84 ± 0.06	15.0719 ± 0.0005	15.2397 ± 0.0043	14.7288 ± 0.0015	DQ	He	6833 ± 24	8.10 ± 0.01	
040026.30+08.1400.8	0357+081	3301319572621418368	53.75 ± 0.05	-362.74 ± 0.12	-394.31 ± 0.07	15.7067 ± 0.0005	16.0887 ± 0.0033	15.1551 ± 0.0024	DA	H	5426 ± 18	7.92 ± 0.01	
041629.95-59.1800.0	0415-594	467866476639382328	54.48 ± 0.05	-45.10 ± 0.08	-175.25 ± 0.09	12.4905 ± 0.0002	12.4099 ± 0.0046	12.5490 ± 0.0030	DA	H	13718 ± 165	7.77 ± 0.02	
042553.63+12.1144.7	0423+120	3307009304776119936	62.38 ± 0.04	-91.34 ± 0.07	-234.29 ± 0.05	15.2812 ± 0.0005	15.5256 ± 0.0045	14.8544 ± 0.0017	DC	He	6129 ± 20	8.20 ± 0.01	
043115.25+5.8581.1	0426+578	470826482635701376	181.28 ± 0.04	+1335.04 ± 0.08	-1947.63 ± 0.09	12.3527 ± 0.0005	12.4942 ± 0.0044	12.0602 ± 0.0014	DC	He	7333 ± 25	8.24 ± 0.01	
043645.16+27.0942.1	0433+030	151650935831913216	57.49 ± 0.06	+227.51 ± 0.12	-148.43 ± 0.09	15.6252 ± 0.0005	15.9911 ± 0.0041	15.0850 ± 0.0019	DA	H	5505 ± 17	8.01 ± 0.01	
043747.66-08.4934.7	0435-088	3186021141200137472	106.27 ± 0.02	+238.35 ± 0.04	-1552.42 ± 0.03	13.6129 ± 0.0002	13.7896 ± 0.0031	13.2440 ± 0.0007	DQ	He	6600 ± 10	8.05 ± 0.01	
050552.64-17.2232.3	0503-174	2982808337003815040	51.67 ± 0.04	+169.41 ± 0.05	+663.76 ± 0.05	15.7960 ± 0.0004	16.1909 ± 0.0042	15.2273 ± 0.0017	DAH	H	5336 ± 15	7.86 ± 0.01	
055119.60-10.0107.6	0548-001	321869776783768320	89.17 ± 0.03	+112.72 ± 0.05	-226.87 ± 0.05	14.4376 ± 0.0004	14.6866 ± 0.0052	14.0032 ± 0.0012	DQP	He	6074 ± 15	8.13 ± 0.01	2
055442.97-10.3523.7		3011223668834627328	65.35 ± 0.03	-64.21 ± 0.06	-152.75 ± 0.06	14.8654 ± 0.0004	15.0668 ± 0.0021	14.4956 ± 0.0016			6692 ± 19	8.24 ± 0.01	
065510.09-10.4043.0	0532-041	3022956969731332096	155.25 ± 0.03	+535.32 ± 0.04	-2316.96 ± 0.04	14.2502 ± 0.0004	14.7607 ± 0.0018	13.6043 ± 0.0010	DZ	H	4883 ± 9	8.16 ± 0.01	
064508.81-16.4319.9	0642-166	2947050466531873024	376.68 ± 0.45	-459.68 ± 0.55	-915.02 ± 0.53	8.4745 ± 0.0020	8.2214 ± 0.0205	8.4827 ± 0.0432	DA	H	27410 ± 4600	8.69 ± 0.20	
064721.72+0.23109.3	0644+025	3126453655659835136	55.25 ± 0.05	-412.14 ± 0.08	+24.88 ± 0.07	15.5990 ± 0.0007	15.7553 ± 0.0037	15.2659 ± 0.0046	DA	H	7093 ± 51	8.59 ± 0.02	
064737.69+37.3042.5	0644+375	943770757800160384	58.57 ± 0.02	-229.73 ± 0.36	-937.76 ± 0.37	12.0714 ± 0.0005	11.9157 ± 0.0072	12.2507 ± 0.0041	DA	H	21071 ± 535	8.13 ± 0.03	
065705.51-39.0938.0	0655-390	5564171814627287296	60.58 ± 0.02	-299.08 ± 0.04	-150.16 ± 0.04	14.9883 ± 0.0003	15.2241 ± 0.0037	14.5703 ± 0.0020	DA	H	6325 ± 22	8.06 ± 0.01	
070052.09+15.734.6	0657+320	890661253803216896	50.97 ± 0.07	+353.90 ± 0.11	-595.56 ± 0.10	16.3478 ± 0.0009	16.8603 ± 0.0137	15.6859 ± 0.0040	DA	H	4821 ± 33	7.87 ± 0.03	
070851.68-67.0632.9	0708-670	5280944182024023552	59.02 ± 0.04	-224.44 ± 0.07	-93.79 ± 0.09	15.9659 ± 0.0006	16.4748 ± 0.0026	15.3175 ± 0.0017	DC	He	4849 ± 10	7.85 ± 0.01	
073303.98+64.0923.4	0728+642	1089400763661597440	49.97 ± 0.05	+42.27 ± 0.06	-257.59 ± 0.06	16.0145 ± 0.0005	16.4586 ± 0.0031	15.4120 ± 0.0024	DAP	H	5126 ± 16	7.81 ± 0.01	
074022.02-1.72457.6	0738-172	5717278911884258176	109.22 ± 0.03	+1138.64 ± 0.04	-560.40 ± 0.08	12.9917 ± 0.0004	13.0924 ± 0.0013	12.7563 ± 0.0007	DZA	He	7978 ± 15	8.13 ± 0.01	
074538.08-33.525.3	0743-336	5586614164276695424	64.78 ± 0.04	-276.18 ± 0.07	+1680.40 ± 0.08	16.2721 ± 0.0006	16.9123 ± 0.0052	15.5093 ± 0.0028	DC	H	4267 ± 22	7.80 ± 0.02	
075015.56+07.1121.3	0747+033	3144837318276010624	54.93 ± 0.07	+11.54 ± 0.13	-1782.66 ± 0.08	16.6084 ± 0.0006	17.2544 ± 0.0051	15.8413 ± 0.0027	DC	H	4241 ± 22	7.76 ± 0.02	
075015.56+07.1109.3	0747+073.1	3144837112117580800	55.14 ± 0.06	+209.90 ± 0.11	-1790.48 ± 0.06	13.7888 ± 0.0003	14.1353 ± 0.0014	15.5093 ± 0.0028	DA	H	5632 ± 8	7.95 ± 0.01	
075312.15-67.4754.5	0752-676	5273943498410008832	122.37 ± 0.01	+1467.07 ± 0.03	-1489.83 ± 0.03	13.7888 ± 0.0003	14.1353 ± 0.0014	13.2728 ± 0.0010	DA	H	4938 ± 11	7.89 ± 0.01	
075356.28-25.3358.3	0751-252	5602379180877207936	56.12 ± 0.08	-297.87 ± 0.13	+206.60 ± 0.26	16.0444 ± 0.0005	16.5334 ± 0.0033	15.4065 ± 0.0014	DA	H	10798 ± 44	8.13 ± 0.01	
080654.62-66.1821.2	0806-661	52745147467840296832	51.93 ± 0.02	-335.55 ± 0.04	-288.89 ± 0.04	13.6826 ± 0.0003	13.6575 ± 0.0029	13.6171 ± 0.0013	DQ	He	6217 ± 9	7.81 ± 0.01	
081226.98-35.2943.8	0810-353	5544743922242648320	89.52 ± 0.02	-66.50 ± 0.03	-29.27 ± 0.03	14.3601 ± 0.0002	14.6150 ± 0.0011	13.9299 ± 0.0011	DC	He	6692 ± 28	8.12 ± 0.01	
081411.27+48.4525.9	0810+489	931573222477949696	58.48 ± 0.04	+65.78 ± 0.06	-253.68 ± 0.04	14.9585 ± 0.0004	15.1466 ± 0.0032	14.6021 ± 0.0021	DC	He	6670 ± 42	8.23 ± 0.01	
081840.55-31.1032.5	0816-310	5548080118389905408	51.65 ± 0.03	+237.72 ± 0.04	-785.98 ± 0.05	15.4077 ± 0.0008	15.6392 ± 0.0046	15.0720 ± 0.0035	DZ	He	4804 ± 10	7.91 ± 0.01	
082125.65-67.0309.8	0821-669	52726990766709543680	93.68 ± 0.02	-397.28 ± 0.05	+660.13 ± 0.05	15.0891 ± 0.0004	15.6071 ± 0.0038	14.4241 ± 0.0028	DA	H	9185 ± 21	7.79 ± 0.01	
084131.12-32.5612.1	0839-327	5639391810273308416	117.33 ± 0.04	+1061.34 ± 0.05	+1345.95 ± 0.06	11.8325 ± 0.0004	11.9021 ± 0.0018	11.6797 ± 0.0009	DA	H	5354 ± 15	8.15 ± 0.01	
084248.18-13.4713.6	0840-136	5734737438536674432	67.55 ± 0.04	-266.03 ± 0.07	-24.95 ± 0.05	15.6081 ± 0.0005	16.0075 ± 0.0031	15.0801 ± 0.0021	DZ	He	4963 ± 18	7.92 ± 0.01	
085913.08-00.05844.7	0856-007	5764485618978306176	54.73 ± 0.07	+156.32 ± 0.11	-119.57 ±								

Table 1: continued.

J2015.5	WD	Gaia DR2 ID	ϖ [mas]	μ_{RA} [mas yr $^{-1}$]	μ_{DEC} [mas yr $^{-1}$]	G [mag]	G_{BP} [mag]	G_{RP} [mag]	G_{RP} [mag]	spType	comp.	T_{eff} [K]	$\log g$ [dex]	Note
091554.19+532506.5	0912+536	1022780838737369216	97.29 ± 0.04	-1086.45 ± 0.10	+1121.31 ± 0.07	13.7945 ± 0.0009	13.9248 ± 0.0043	13.5168 ± 0.0055	13.5168 ± 0.0055	DGP	He	7428 ± 70	8.33 ± 0.01	
100149.00+144124.0	0959+149	615735395893566317	51.53 ± 0.07	-338.68 ± 0.18	+111.11 ± 0.26	15.3232 ± 0.0006	15.5052 ± 0.0028	14.9724 ± 0.0020	14.9724 ± 0.0020	DC	He	6748 ± 28	8.20 ± 0.01	4
101141.43+284548.0	1008+290	740483560857296768	67.79 ± 0.08	-124.78 ± 0.12	-713.28 ± 0.11	16.5628 ± 0.0013	17.3209 ± 0.0315	15.6678 ± 0.0026	15.6678 ± 0.0026	DQpecP	He	3905 ± 20	7.60 ± 0.02	
101201.30+184333.5	1009+184	5669427512997660800	55.27 ± 0.06	-522.26 ± 0.08	-12.89 ± 0.08	15.3467 ± 0.0007	15.5827 ± 0.0026	14.9641 ± 0.0027	14.9641 ± 0.0027	DA	He	6349 ± 25	8.16 ± 0.01	
102309.76+632744.9	1019+637	1052520154368111872	62.73 ± 0.02	+229.99 ± 0.03	+222.01 ± 0.04	14.6065 ± 0.0003	14.8012 ± 0.0030	14.2472 ± 0.0014	14.2472 ± 0.0014	DA	H	6789 ± 19	8.03 ± 0.01	
103656.53+711051.5	1033+714	1076941716370493696	56.70 ± 0.06	-1857.35 ± 0.08	-463.47 ± 0.10	16.6271 ± 0.0008	17.1712 ± 0.0064	15.9318 ± 0.0031	15.9318 ± 0.0031	DC	H	4658 ± 24	8.13 ± 0.01	
103855.25+200648.3	1036+204	3553682127126319360	70.76 ± 0.08	-287.98 ± 0.10	+551.28 ± 0.09	15.8614 ± 0.0016	16.0458 ± 0.0261	15.3476 ± 0.0025	15.3476 ± 0.0025	DQpecP	He	5534 ± 29	8.47 ± 0.01	
104537.90+190654.4	1043+188	3554395813252626048	53.13 ± 0.06	-1867.35 ± 0.10	-604.03 ± 0.07	15.4552 ± 0.0009	15.7185 ± 0.0068	14.9261 ± 0.0025	14.9261 ± 0.0025	DQpec	He	5756 ± 56	7.89 ± 0.03	
105734.28+073121.8	1055-072	3763445409285757824	81.46 ± 0.04	-817.04 ± 0.06	+91.30 ± 0.05	14.2576 ± 0.0004	14.3855 ± 0.0026	13.9708 ± 0.0017	13.9708 ± 0.0017	DC	He	7399 ± 28	8.37 ± 0.01	
111826.69+127156.4	1116+470	5374565879145559424	58.71 ± 0.04	-331.33 ± 0.05	+34.32 ± 0.05	15.3800 ± 0.0005	15.6542 ± 0.0035	14.9216 ± 0.0013	14.9216 ± 0.0013	DC	He	5907 ± 15	8.08 ± 0.01	
113429.61+324949.6	1132+325	3478127467639543296	104.74 ± 0.07	-701.62 ± 0.12	+828.82 ± 0.09	14.5589 ± 0.0009	14.9211 ± 0.0040	13.9860 ± 0.0030	13.9860 ± 0.0030	DC	He	5407 ± 22	8.12 ± 0.01	
113704.93+294758.1	1134+300	4019458647338779648	63.78 ± 0.09	-147.46 ± 0.10	-12.78 ± 0.12	12.5093 ± 0.0006	12.3713 ± 0.0060	12.6967 ± 0.0017	12.6967 ± 0.0017	DA	H	21949 ± 248	8.55 ± 0.01	
114549.39+645034.8	1142-645	5332066622595645952	215.74 ± 0.03	+2661.59 ± 0.05	-344.85 ± 0.05	11.4318 ± 0.0004	11.5072 ± 0.0045	11.2352 ± 0.0009	11.2352 ± 0.0009	DQ	He	8540 ± 23	8.23 ± 0.01	2
114730.70+745738.2	1147-645	5224999346778496128	50.10 ± 0.08	-1067.75 ± 0.13	+135.84 ± 0.12	17.1756 ± 0.0009	17.9375 ± 0.0145	16.3476 ± 0.0042	16.3476 ± 0.0042	DQ	He	3711 ± 82	7.67 ± 0.05	
115052.40+683115.3	1148+687	1058284412796260480	58.51 ± 0.03	+23.39 ± 0.05	-41.17 ± 0.05	15.1418 ± 0.0004	15.3456 ± 0.0029	14.7707 ± 0.0022	14.7707 ± 0.0022	DA	H	6678 ± 25	8.26 ± 0.01	
120526.72+223308.6	1202-232	3489719481290397696	95.84 ± 0.05	+41.77 ± 0.07	+226.62 ± 0.06	12.7548 ± 0.0002	12.8435 ± 0.0021	12.5587 ± 0.0007	12.5587 ± 0.0007	DAZ	H	8652 ± 15	7.99 ± 0.01	
121130.07+572411.5	1208+576	1575357587146077056	50.10 ± 0.03	+413.77 ± 0.05	-369.07 ± 0.04	15.6350 ± 0.0005	15.9464 ± 0.0026	15.1411 ± 0.0019	15.1411 ± 0.0019	DAZ	H	5797 ± 15	7.97 ± 0.01	
122641.94+661221.3	1223-659	5860131207828395648	64.97 ± 0.02	-33.74 ± 0.03	-182.86 ± 0.03	13.9355 ± 0.0004	14.0717 ± 0.0031	13.6573 ± 0.0011	13.6573 ± 0.0011	DA	H	7615 ± 21	7.91 ± 0.01	
123848.89+494801.4	1236-495	6127333286605955072	67.52 ± 0.04	-557.23 ± 0.07	-74.09 ± 0.04	13.8113 ± 0.0003	13.8068 ± 0.0026	13.7783 ± 0.0011	13.7783 ± 0.0011	DAV	H	11527 ± 40	8.71 ± 0.01	
130008.61+032827.6	1257+037	3704392873140270336	60.80 ± 0.20	-439.16 ± 0.72	-865.95 ± 0.19	15.6477 ± 0.0005	15.9989 ± 0.0048	15.1286 ± 0.0017	15.1286 ± 0.0017	DAV	H	5632 ± 16	8.19 ± 0.01	
130843.76+850224.3	1309+853	1726678630833373824	60.72 ± 0.04	+214.28 ± 0.07	-250.83 ± 0.06	15.8209 ± 0.0006	16.2435 ± 0.0055	15.2354 ± 0.0024	15.2354 ± 0.0024	DAP	H	5240 ± 20	8.07 ± 0.01	
131253.16+472802.9	1310-472	6085402414245451520	59.55 ± 0.18	-2165.62 ± 0.16	-60.91 ± 0.17	16.7080 ± 0.0007	17.4131 ± 0.0145	15.8764 ± 0.0039	15.8764 ± 0.0039	DC	H	3765 ± 68	7.64 ± 0.05	
131924.74+214802.0	1316-211	3506061587037686144	50.48 ± 0.10	-4.39 ± 0.18	-460.43 ± 0.21	16.5490 ± 0.0003	16.8657 ± 0.0057	16.0636 ± 0.0048	16.0636 ± 0.0048	DA	H	5845 ± 38	8.60 ± 0.01	4
131927.10+782333.7	1315-781	5787859896160384384	51.84 ± 0.04	+300.04 ± 0.07	-356.51 ± 0.06	15.9752 ± 0.0005	16.3455 ± 0.0041	15.4453 ± 0.0019	15.4453 ± 0.0019	DC	H	5552 ± 17	8.13 ± 0.01	
133012.48+083436.8	1327-083	363003578792473600	62.19 ± 0.09	-1111.14 ± 0.13	-472.38 ± 0.12	12.3765 ± 0.0006	12.3246 ± 0.0041	12.4653 ± 0.0015	12.4653 ± 0.0015	DA	H	14808 ± 113	7.99 ± 0.01	
134121.35+050046.1	1338+052	37149142271705535360	68.20 ± 0.07	-429.82 ± 0.15	+18.84 ± 0.10	16.3308 ± 0.0009	17.0291 ± 0.0055	15.5335 ± 0.0031	15.5335 ± 0.0031	DC	H	4030 ± 28	7.75 ± 0.02	
134801.34+233448.4	1345+238	1251824057289839744	84.27 ± 0.04	-1485.68 ± 0.06	+125.12 ± 0.05	15.3520 ± 0.0004	15.9235 ± 0.0021	14.6393 ± 0.0017	14.6393 ± 0.0017	DA	H	4558 ± 10	7.75 ± 0.01	
135315.90+091638.9	1350-090	3618657732410663808	50.73 ± 0.04	+352.09 ± 0.08	-358.63 ± 0.06	14.5687 ± 0.0006	14.6423 ± 0.0021	14.3872 ± 0.0014	14.3872 ± 0.0014	DAP	H	8836 ± 32	8.32 ± 0.01	4
141159.33+592045.9	1411-33	586776696271127424	69.48 ± 0.04	+79.27 ± 0.06	-59.72 ± 0.08	14.5635 ± 0.0003	14.7656 ± 0.0028	14.1856 ± 0.0011	14.1856 ± 0.0011	DC	H	6641 ± 15	8.10 ± 0.01	5
144724.15+174221.1	1444-174	6282457918962299776	75.17 ± 0.07	-1098.57 ± 0.12	-343.06 ± 0.09	16.1723 ± 0.0011	16.6647 ± 0.0110	15.5308 ± 0.0035	15.5308 ± 0.0035	DC	H	4940 ± 30	8.43 ± 0.02	
153505.63+112741.4	1532+129	1193520666521113344	51.90 ± 0.06	-165.59 ± 0.08	-179.71 ± 0.08	15.6030 ± 0.0012	15.9664 ± 0.0067	15.1388 ± 0.0022	15.1388 ± 0.0022	DZ	He	5787 ± 25	7.99 ± 0.01	
154729.47+375511.7	1544-377	6009537829925128064	65.63 ± 0.05	-423.55 ± 0.10	-209.21 ± 0.06	13.0177 ± 0.0005	13.0251 ± 0.0027	12.9355 ± 0.0011	12.9355 ± 0.0011	DA	H	10355 ± 33	8.02 ± 0.01	
162333.34+391346.2	1620-391	6018034958869558912	77.43 ± 0.07	+77.14 ± 0.15	+0.33 ± 0.11	10.9964 ± 0.0014	10.8557 ± 0.0081	11.2314 ± 0.0019	11.2314 ± 0.0019	DA	H	25813 ± 375	8.08 ± 0.02	
162824.37+386427.4	1626+368	1331106782752978688	62.91 ± 0.02	-494.19 ± 0.03	+746.55 ± 0.04	13.8013 ± 0.0003	13.8340 ± 0.0046	13.6682 ± 0.0012	13.6682 ± 0.0012	DZA	He	9527 ± 34	8.26 ± 0.01	
163233.46+085118.7	1630+089	4440264291578812928	77.38 ± 0.03	+278.02 ± 0.04	-259.03 ± 0.02	14.9064 ± 0.0002	15.2574 ± 0.0013	14.3820 ± 0.0007	14.3820 ± 0.0007	DA	He	5596 ± 6	8.02 ± 0.01	
163419.43+571027.5	1633+572	1431176943768691328	67.32 ± 0.02	-1180.87 ± 0.05	+119.40 ± 0.04	14.8616 ± 0.0004	15.1154 ± 0.0029	14.4324 ± 0.0005	14.4324 ± 0.0005	DQ	He	6106 ± 16	8.02 ± 0.01	
163501.75+431731.7	1633+433	1405343643196929536	68.97 ± 0.02	+226.17 ± 0.03	-301.78 ± 0.03	14.7301 ± 0.0003	14.9522 ± 0.0027	14.3365 ± 0.0018	14.3365 ± 0.0018	DAZ	H	6498 ± 20	8.15 ± 0.01	
164825.90+590318.0	1647+591	1431783457574556672	91.41 ± 0.04	+131.55 ± 0.06	-298.05 ± 0.10	12.2913 ± 0.0005	12.2719 ± 0.0031	12.3032 ± 0.0014	12.3032 ± 0.0014	DAV	H	12364 ± 64	8.30 ± 0.01	
170641.33+544336.2	1705+030	4108828945319007744	76.62 ± 0.06	-25.75 ± 0.09	-95.51 ± 0.05	15.0184 ± 0.0007	15.2767 ± 0.0039	14.5731 ± 0.0031	14.5731 ± 0.0031	DZ	He	6152 ± 28	8.35 ± 0.01	2
170807.95+025730.9	1705+037	4388138816124225792	55.97 ± 0.03	-11.89 ± 0.06	-397.80 ± 0.04	15.1107 ± 0.0003	15.2946 ± 0.0026	14.7843 ± 0.0015	14.7843 ± 0.0015	DZ	He	6930 ± 22	8.24 ± 0.01	
174736.13+543635.9	1743-545	592090901901635968	73.98 ± 0.07	-383.95 ± 0.10	-306.68 ± 0.08	15.9489 ± 0.0008	16.5473 ± 0.0111	15.1990 ± 0.0017	15.1990 ± 0.0017	DC	H	4336 ± 18	7.81 ± 0.01	
174804.00+705253.1	1748+708	1638979384378696704	160.98 ± 0.01	-1266.42 ± 0.03	+1108.87 ± 0.03	13.7887 ± 0.0003	14.1827 ± 0.0043	13.1882 ± 0.0010	13.1882 ± 0.0010	DXP	He	5088 ± 8	8.03 ± 0.01	
174938.34+824717.4	1756+827	1711005951573009792	61.16 ± 0.02	-1436.86 ± 0.03	+3314.40 ± 0.03	14.2305 ± 0.0003	14.3906 ± 0.0031	13.9155 ± 0.0020	13.9155 ± 0.0020	DA	H	7201 ± 30	7.87 ± 0.01	
181706.03+132807.7	1814+134	4497414466452138496	66.07 ± 0.05	-436.06 ± 0.08	-1115.45 ± 0.09	15.6284 ± 0.0006	16.1431 ± 0.0026	14.9696 ± 0.0024	14.9696 ± 0.0024	DA	H	4816 ± 13	7.77 ± 0.01	
182120.15+610056.6	1820+609	2158285185808357504	72.92 ± 0.03	+147.90 ± 0.06	-698.53 ± 0.05	15.4131 ± 0.0005	15.9250 ± 0.0057	14.7461 ± 0.0014	14.7461 ± 0.0014	DA	H	4796 ± 12	7.75 ± 0.01	
182404.33+130852.2	1821-131	4152557420406043264	52.38 ± 0.06	-205.47 ± 0.10	-638.93 ± 0.08	15.4109 ± 0.0006	15.6871 ± 0.0053	14.9539 ± 0.0026	14.9539 ± 0.0026	DAZ	H	6037 ± 27	8.00 ± 0.01	
182425.90+135558.0	1821-131	4484184592790777728	50.91 ± 0.07	-326.68 ± 0.12	+45.23 ± 0.11	16.3112 ± 0.0001	16.8230 ± 0.0060	15.6607 ± 0.0049	15.6607 ± 0.0049	DAZ	H	4847 ± 29	7.87 ± 0.03	2
183019.79+544731.7	1829+547	2150504594853811456	58.70 ± 0.03	-267.07 ± 0.06	+287.62 ± 0.06	15.4668 ± 0.0005	15.6760 ± 0.0026	15.0977 ± 0.0021	15.0977 ± 0.0021	DXP	He	6536 ± 24	8.40 ± 0.01	
190010.52+703959.2	1900+705	2262849634963004416	77.65 ± 0.03	+85.77 ± 0.05	+505.05 ± 0.07	13.2644 ± 0.0004	13.2033 ± 0.0050	13.2532 ± 0.0022	13.2532 ± 0.0022	DAP	He	12140 ± 90	8.64 ± 0.01	
191858.66+384317.6	1917+386	2052891361294411520	84.21 ± 0.02	+25.12 ± 0.04	-251.60 ± 0.04	14.4803 ± 0.0003	14.7274 ± 0.0122	14.0780 ± 0.0011	14.0780 ± 0.0011	DC	He	6299 ± 13	8.17 ± 0.01	
192034.86+074002.6	1917-077	420178169694073472	95.25 ± 0.0											

Table 1: continued.

J2015.5	WD	<i>Gai</i> a DR2 ID	ϖ [mas]	μ_{Ra} [mas yr ⁻¹]	μ_{Dec} [mas yr ⁻¹]	<i>G</i> [mag]	<i>G</i> _{BP} [mag]	<i>G</i> _{RP} [mag]	<i>G</i> _{RP} [mag]	spType	comp.	<i>T</i> _{eff} [K]	log <i>g</i> [dex]	Note
203421.42+250341.0	2032+248	1831553382794173824	67.49 ± 0.06	-403.63 ± 0.08	-563.33 ± 0.09	11.5514 ± 0.0009	11.4206 ± 0.0056	11.7246 ± 0.0012	11.7246 ± 0.0012	DA	H	20290 ± 196	7.95 ± 0.01	
204421.96+680524.9	2039-682	6424566979354709248	50.98 ± 0.05	+182.09 ± 0.06	-228.21 ± 0.08	13.3566 ± 0.0003	13.2784 ± 0.0035	13.4757 ± 0.0010	13.4757 ± 0.0010	DA	H	16877 ± 96	8.49 ± 0.01	
204906.91+372816.3	2047+372	1871118140493076224	56.90 ± 0.04	+162.01 ± 0.06	+148.05 ± 0.06	13.0563 ± 0.0005	13.0007 ± 0.0026	13.1349 ± 0.0012	13.1349 ± 0.0012	DA	H	14700 ± 78	8.30 ± 0.01	
205020.17+263036.1	2048+263	1844125748497557632	52.35 ± 0.05	-414.92 ± 0.07	-300.95 ± 0.05	15.4043 ± 0.0004	15.8997 ± 0.0029	14.7619 ± 0.0017	14.7619 ± 0.0017	DA	H	4895 ± 12	7.27 ± 0.01	
205213.51+250417.5		6805792571514600960	55.65 ± 0.06	+86.82 ± 0.09	-152.91 ± 0.07	16.0418 ± 0.0006	16.5427 ± 0.0038	15.4009 ± 0.0022	15.4009 ± 0.0022	DC	H	4907 ± 15	7.85 ± 0.01	2
205648.59-045043.0	2054-050	6913810483611035776	61.75 ± 0.07	+776.36 ± 0.11	-222.94 ± 0.07	16.3629 ± 0.0005	16.9687 ± 0.0049	15.6187 ± 0.0022	15.6187 ± 0.0022	DC	H	4383 ± 18	7.86 ± 0.01	
211014.75-490627.8	2057-493	6478328218869704192	74.89 ± 0.04	-286.96 ± 0.05	-226.36 ± 0.05	15.2756 ± 0.0004	15.7226 ± 0.0027	14.6678 ± 0.0014	14.6678 ± 0.0014	DA	H	5111 ± 11	7.92 ± 0.01	
211318.77-814918.8	2105-820	6348672845649310464	61.86 ± 0.03	+264.23 ± 0.06	-379.98 ± 0.06	13.6243 ± 0.0003	13.6677 ± 0.0031	13.5208 ± 0.0012	13.5208 ± 0.0012	DAZH	H	10055 ± 33	8.27 ± 0.01	
211856.11+541244.2	2117+539	217611658005936512	57.87 ± 0.04	-85.51 ± 0.07	+193.33 ± 0.07	12.4078 ± 0.0003	12.3450 ± 0.0018	12.5000 ± 0.0006	12.5000 ± 0.0006	DA	H	14942 ± 49	7.92 ± 0.01	
214157.34-330031.6	2138-332	6592315723192176896	62.07 ± 0.04	-181.46 ± 0.05	-113.31 ± 0.04	14.4638 ± 0.0005	14.6412 ± 0.0035	14.1997 ± 0.0024	14.1997 ± 0.0024	DZ	He	7423 ± 38	8.13 ± 0.01	
214240.76+205948.1	2140+207	1792830060723673472	90.64 ± 0.03	-224.66 ± 0.05	-649.62 ± 0.05	13.1948 ± 0.0006	13.2453 ± 0.0051	13.0274 ± 0.0017	13.0274 ± 0.0017	DQ	He	8969 ± 43	8.25 ± 0.01	
214324.08-065949.4		2667464656943675392	55.11 ± 0.05	-11.19 ± 0.08	-91.66 ± 0.08	14.5429 ± 0.0007	14.6069 ± 0.0057	14.3659 ± 0.0025	14.3659 ± 0.0025	H	H	8961 ± 61	8.44 ± 0.01	2
215139.93+591734.6		2202703050401536000	118.12 ± 0.02	-86.80 ± 0.04	-19.19 ± 0.04	14.3852 ± 0.0003	14.8319 ± 0.0019	13.7723 ± 0.0012	13.7723 ± 0.0012	DQP	He	5095 ± 8	7.98 ± 0.01	
215738.28-510037.7	2154-512	6558209044297239424	67.25 ± 0.03	-46.19 ± 0.04	-397.39 ± 0.04	14.5302 ± 0.0004	14.6951 ± 0.0062	14.1414 ± 0.0020	14.1414 ± 0.0020	DA	H	6460 ± 27	7.93 ± 0.01	
220418.72-751324.9	2159-754	6358158435541361792	52.48 ± 0.03	-527.67 ± 0.05	+74.23 ± 0.05	15.0071 ± 0.0004	15.0749 ± 0.0029	14.8302 ± 0.0015	14.8302 ± 0.0015	DA	H	8951 ± 37	8.64 ± 0.01	
221436.10-385913.0	2211-392	657378541262656256	55.09 ± 0.10	+1011.62 ± 0.10	-368.54 ± 0.09	15.7953 ± 0.0007	16.0783 ± 0.0040	15.3507 ± 0.0021	15.3507 ± 0.0021	DA	H	6105 ± 22	8.37 ± 0.01	
223035.20-751552.6	2226-754	6357629089412187648	66.53 ± 0.05	+409.50 ± 0.09	-1827.90 ± 0.09	16.4606 ± 0.0007	17.1929 ± 0.0064	15.6408 ± 0.0033	15.6408 ± 0.0033	DC	H	3848 ± 31	7.69 ± 0.03	
223041.65-751423.5	2226-755	6357630601240673792	66.45 ± 0.04	+410.98 ± 0.08	-1825.78 ± 0.08	16.2012 ± 0.0007	16.8661 ± 0.0053	15.4296 ± 0.0028	15.4296 ± 0.0028	DC	H	4193 ± 23	7.73 ± 0.02	
224906.14+223632.9	2246+223	283660909335562496	56.12 ± 0.07	+522.74 ± 0.12	+59.63 ± 0.07	14.3899 ± 0.0003	14.4116 ± 0.0023	14.3093 ± 0.0021	14.3093 ± 0.0021	DA	H	10491 ± 57	8.66 ± 0.01	
225124.51+293946.6	2248+293	1884744525522874880	51.47 ± 0.14	+1250.15 ± 0.17	+135.20 ± 0.19	15.3513 ± 0.0004	15.6959 ± 0.0018	14.8328 ± 0.0017	14.8328 ± 0.0017	DA	H	5613 ± 12	7.71 ± 0.01	
225355.97-064705.0	2251-070	2611561706216413696	117.15 ± 0.05	+2485.85 ± 0.09	-681.21 ± 0.09	15.4377 ± 0.0008	16.1182 ± 0.0039	14.6697 ± 0.0032	14.6697 ± 0.0032	DZ	He	4239 ± 15	8.02 ± 0.02	
230959.27+550650.2	2307+548	1996725077535283200	60.91 ± 0.04	+407.33 ± 0.06	+47.98 ± 0.06	15.6154 ± 0.0005	15.9761 ± 0.0044	15.0746 ± 0.0031	15.0746 ± 0.0031	DA	H	5517 ± 24	8.10 ± 0.01	
232847.22+051450.1	2326+049	2660358032257156736	57.02 ± 0.06	-398.20 ± 0.12	-266.74 ± 0.08	13.0885 ± 0.0031	13.0827 ± 0.0104	13.0618 ± 0.0064	13.0618 ± 0.0064	DAZV	H	11295 ± 214	8.02 ± 0.03	
233850.77-074120.3	2336-079	2439184703619919488	53.59 ± 0.04	+31.56 ± 0.08	-22.30 ± 0.06	13.3111 ± 0.0004	13.3206 ± 0.0026	13.2654 ± 0.0013	13.2654 ± 0.0013	DA	H	10940 ± 39	8.03 ± 0.01	
234350.46+323245.8	2341+322	2871730307948650368	53.70 ± 0.09	-215.82 ± 0.17	-59.74 ± 0.07	12.9886 ± 0.0005	12.9660 ± 0.0022	13.0154 ± 0.0007	13.0154 ± 0.0007	DA	H	12605 ± 44	8.01 ± 0.01	

Notes: (1) For our model atmosphere fits, $\log(\text{H}/\text{He}) = -1$ and -3 were assumed for WD 0038-226 and WD 2008-600 respectively. (2) Newly identified white dwarf. (3) The $\text{PHOT_BP_RP_EXCESS_FACTOR}$ value of 1.661 indicates that the modelling of the background flux is not good enough to fit the *Gai*a fluxes. (4) Known white dwarf, but not previously considered a potential 20 pc member. (5) White dwarf candidate recently identified by Smith et al. (2018) via its proper-motion.

Table 2: White dwarfs previously thought to reside within 20 pc that are now confirmed to be outside the 20 pc sample. The reference column indicates the source of the previous parallax/distance estimate. The 0.03 mas offset (Lindgren et al. 2018) is not included in ϖ_{DR2} , but is folded into the calculation of D_{DR2} .

J2015.5	WD	Gaia DR2 ID	ϖ_{DR2} [mas]	D_{DR2} [pc]	ϖ_{old} [mas]	D_{old} [pc]	Ref.
000754.60+394731.0	0005+395	383108338321272448	29.038 ± 0.064	34.402 ± 0.075		20.2 ± 4.2	1
002214.93+423638.0	0019+423	385105360675267840	29.318 ± 0.060	34.074 ± 0.070	42 ± 4	23.8 ± 2.3	2
002640.19-552451.1	0024-556	4920057871348614272	41.553 ± 0.032	24.049 ± 0.019		19	3
010350.26+050434.2	0101+048	2552121179905893888	44.864 ± 0.119	22.275 ± 0.059	46.9 ± 3.8	21.3 ± 1.7	4
011044.51+275813.3	0108+277	307323228064848512	26.347 ± 0.112	37.912 ± 0.161		26.6 ± 4.4	1
021616.14+395123.9	0213+396	332820971434386432	49.077 ± 0.041	20.364 ± 0.017	50.75 ± 0.82	19.70 ± 0.32	5
021659.23+425756.2	0213+427	351429930856438656	48.889 ± 0.094	20.442 ± 0.039	50.2 ± 4.1	19.9 ± 1.7	4
023407.98-051137.9	0231-054	2488960249844340352	41.628 ± 0.055	24.005 ± 0.032	55.0 ± 10.4	18.2 ± 3.6	6
024631.03-022731.1	0243-026	2495751967528809216	46.603 ± 0.109	21.444 ± 0.050	50.11 ± 1.27	19.96 ± 0.51	5
025617.25+495439.0	0252+497	439494077735062144	26.566 ± 0.094	37.600 ± 0.133		17.99 ± 2.90	7
034323.20+195816.1	0340+198	63126196662620416	48.140 ± 0.062	20.760 ± 0.027		22.8 ± 1.2	1
034707.07+013841.3	0344+014	3270079526697712768	49.621 ± 0.069	20.141 ± 0.028	50.46 ± 1.07	19.83 ± 0.42	5
041805.48+421058.9	0414+420	229143725086190336	33.717 ± 0.097	29.632 ± 0.085		23.8 ± 5.1	1
042105.61-483915.3	0419-487	4788741548375134336	47.160 ± 0.024	21.191 ± 0.011	49.68 ± 1.34	20.14 ± 0.54	8
054458.81+260238.6	0541+260	3429296884940000000	27.681 ± 0.102	36.087 ± 0.133		22.4 ± 4.5	1
062048.31+064516.9	0618+067	3324181683539044224	41.473 ± 0.104	24.094 ± 0.060	44.2 ± 4.2	22.7 ± 2.2	4
062141.77-401624.4	0620-402	5573532025833121408	42.268 ± 0.042	23.642 ± 0.023		25.3 ± 4.0	9
063038.48-020553.2	0628-020	3117320802840630400	46.707 ± 0.036	21.396 ± 0.016	46.51 ± 1.76	21.53 ± 0.82	8
065350.12+635551.9	0649+639	1100267237077449728	35.957 ± 0.057	27.788 ± 0.044		20.8 ± 1.1	1
080556.85+383336.1	0802+387	908962109449446656	48.459 ± 0.090	20.623 ± 0.038	49.06 ± 0.56	20.38 ± 0.23	5
083039.28+324139.1	0827+328	710766750855439360	44.721 ± 0.058	22.346 ± 0.029	44.9 ± 3.8	22.3 ± 1.9	4
083758.73-501743.1	0836-501	5322090003089341440	31.533 ± 0.033	31.683 ± 0.034	43.1 ± 5.2	23.2 ± 2.8	6
085914.31+325712.1	0856+331	712888090655562624	43.363 ± 0.051	23.045 ± 0.027	48.8 ± 3.4	20.5 ± 1.4	4
095016.69+531514.3	0946+534	1020653077580086784	36.308 ± 0.048	27.520 ± 0.036	43.5 ± 3.5	23.0 ± 1.9	4
095748.04+243250.7	0955+247	642685200933153408	36.271 ± 0.063	27.547 ± 0.048	40.9 ± 4.5	24.4 ± 2.7	4
110759.89-050932.9	1105-048	3788194488314248832	40.281 ± 0.078	24.807 ± 0.048	50 ± 10	20 ± 4	2
114544.10+630553.8	1143+633	863131372427958912	41.641 ± 0.049	23.997 ± 0.028	47.0 ± 5.0	21.3 ± 2.3	2
114802.47-452307.5	1145-451	5377849123945711872	39.858 ± 0.050	25.070 ± 0.032		22.94 ± 2.08	7
121651.19+025806.7	1214+032	3701290326205270528	42.784 ± 0.063	23.357 ± 0.035	46.0 ± 3.4	21.7 ± 1.6	2
131258.28+580510.0	1310+583	1566603962760532736	31.322 ± 0.238	31.896 ± 0.242		23.2 ± 0.8	1
134200.00-341501.7	1339-340	6165095738576250624	48.220 ± 0.118	20.725 ± 0.051	47.62 ± 0.93	21.00 ± 0.41	5
134723.43+102135.8	1344+106	3725570772761744384	48.079 ± 0.042	20.786 ± 0.018	49.9 ± 3.6	20.0 ± 1.5	4
152621.16+293625.4	1524+297	1273685372108354176	43.128 ± 0.051	23.171 ± 0.027		22.4 ± 3.7	1
154234.69+232935.2	1540+236	1218051664291152000	36.023 ± 0.067	27.737 ± 0.052		19.6 ± 0.8	1
161125.62+132209.5	1609+135	4458207634145130368	44.849 ± 0.049	22.282 ± 0.024	54.5 ± 4.7	18.3 ± 1.6	4
162753.39+091208.7	1625+093	4452521234885949184	39.879 ± 0.049	25.057 ± 0.031	42.8 ± 3.7	23.4 ± 2.0	4
163441.93+173633.6	1632+177	4466388790929771904	39.047 ± 0.033	25.590 ± 0.022		19.0 ± 0.9	1
163854.15+054035.8	1636+057	4435778215414219520	27.779 ± 0.063	35.959 ± 0.081		20	3
164056.94+534106.4	1639+537	1425909733315616000	49.652 ± 0.030	20.128 ± 0.012	47.4 ± 3.5	21.1 ± 1.6	4
165709.89+212639.8	1655+215	4565048312887877888	47.597 ± 0.024	20.996 ± 0.011	43.0 ± 3.1	23.3 ± 1.7	4
184257.50-110857.1	1840-111	4107012041007171456	41.440 ± 0.049	24.114 ± 0.029	53.0 ± 6.0	18.9 ± 2.2	2
184325.59+042023.9	1840+042	4280632829779587072	40.211 ± 0.040	24.850 ± 0.025	40.2 ± 3.4	24.9 ± 2.1	4
201355.41+064235.8	2011+065	4249667902270614272	43.618 ± 0.047	22.911 ± 0.025	44.7 ± 1.9	22.4 ± 1.0	4
204235.15-200437.4	2039-202	6857939315643803776	46.112 ± 0.073	21.672 ± 0.034	48.22 ± 3.77	20.7 ± 1.6	10
205945.39+551736.5	2058+550	2188860027203347968	44.070 ± 0.075	22.676 ± 0.038		22.6 ± 3.6	1
211329.26+072706.0	2110+072	1739921801713625600	34.092 ± 0.065	29.307 ± 0.056	41.1 ± 3.8	24.3 ± 2.3	4
212657.86+733839.8	2126+734A	2274076297221555968	45.043 ± 0.038	22.186 ± 0.019	47.1 ± 2.4	21.2 ± 1.1	4
212657.96+733838.0	2126+734B	2274076301516712704	45.145 ± 0.211	22.136 ± 0.103	47.1 ± 2.4	21.2 ± 1.1	4
215406.46-011713.6	2151-015	2679976510857026048	39.229 ± 0.133	25.472 ± 0.086	51 ± 6	19.6 ± 2.3	2
221154.36+564948.8	2210+565	2198431172852758656	26.414 ± 0.036	37.816 ± 0.051		22.3 ± 1.4	1
221748.21+370752.3	2215+368	1907041590544054656	49.133 ± 0.079	20.341 ± 0.033	49.19 ± 0.28	20.33 ± 0.12	5
231023.04-685019.0	2307-691	6387649708219253248	47.414 ± 0.036	21.077 ± 0.016	47.75 ± 0.87	20.94 ± 0.38	10
232520.24+140341.4	2322+137	2813020961166816512	42.339 ± 0.126	23.602 ± 0.070	44.9 ± 2.0	22.3 ± 1.0	11
233536.72-161745.9	2333-165	2395444208921491456	41.021 ± 0.050	24.360 ± 0.030	41.6 ± 4.1	24.0 ± 2.4	6
234735.31+030435.5	2345+027	2742789930821144320	39.739 ± 0.077	25.145 ± 0.049		22.7 ± 3.6	1
234954.96+293356.2	2347+292	2867032958053059200	47.741 ± 0.050	20.933 ± 0.022	46.5 ± 4.1	21.5 ± 1.9	4
235400.69-331637.3	2351-335	2313836325604479616	43.124 ± 0.032	23.173 ± 0.017	42.82 ± 2.40	23.35 ± 1.32	8

References: (1) Limoges et al. (2015), (2) Gliese & Jahreiß (1991), (3) Gianninas et al. (2011), (4) van Altena et al. (1995), (5) Subasavage et al. (2017), (6) Finch et al. (2018), (7) Holberg et al. (2016) (8) Subasavage et al. (2009), (9) Subasavage et al. (2008), (10) van Leeuwen (2007), (11) Lépine et al. (2009).

Table 3: Rejected white dwarf candidates from our selection of 20 pc sources. The parallaxes and proper motions are the *Gaia* measurements irrespective of whether they are considered to be correct. AEM is the astrometric excess noise. The T_{eff} and $\log g$ are from our fits to the absolute photometry of *Gaia* and where available Pan-STARRS and 2MASS, *assuming* a white dwarf with a hydrogen dominated atmosphere.

<i>Gaia</i> DR2 ID	ϖ [mas]	μ_{Ra} [mas yr $^{-1}$]	μ_{Dec} [mas yr $^{-1}$]	AEM [mas]	T_{eff} [K]	$\log g$	Note
1474900771698364672	64.99 ± 0.48	-26.26 ± 0.37	-22.85 ± 0.24	0.80	5357 ± 13	8.14 ± 0.01	1
3456953931703563264	68.57 ± 0.76	$+1.33 \pm 0.41$	$+0.09 \pm 0.31$	0.48	4532 ± 18	7.42 ± 0.01	2
4519850409232889856	53.54 ± 0.28	-19.61 ± 0.21	-116.96 ± 0.48	0.77	3248 ± 285	6.45 ± 0.01	3
6031231499269624832	55.72 ± 0.23	$+37.66 \pm 0.53$	$+29.80 \pm 0.21$	0.35	4375 ± 8	6.62 ± 0.01	4
6206558253342895488	60.44 ± 0.60	$+71.09 \pm 0.82$	-54.16 ± 0.56	0.62	4852 ± 57	8.59 ± 0.01	5
6432981674985955584	59.41 ± 0.20	-39.70 ± 0.21	-2.44 ± 0.34	0.36	5988 ± 5	6.66 ± 0.01	6

Notes: (1) Atypically large astrometric noise, low proper motion, and infrared photometry that is inconsistent with the optical fit. (2) Extremely small proper motion and moderate astrometric noise. (3) Infrared 2MASS photometry suggests a cool main-sequence object. Furthermore, the low PPMXL proper motion value of $(\mu_{\text{Ra}}, \mu_{\text{Dec}}) = (-5.2, +3.9) \pm 3.8$ mas yr $^{-1}$ is inconsistent with *Gaia* DR2. (4) Low proper motion, moderate astrometric noise and low measured $\log g$ assuming a white dwarf. The even lower PPMXL proper motion of $(+3.4, -10.3) \pm 4.0$ mas yr $^{-1}$ is discrepant with *Gaia* DR2. (5) The proper-motion is inconsistent with data from elsewhere calling into question the accuracy of the parallax (see Section 2.2). Furthermore this star appears very close to a much brighter B-type star. (6) Low proper motion and low $\log g$ required to fit the photometry and parallax. The very low PPMXL proper-motion of $(+4.9, -1.6) \pm 7.3$ mas yr $^{-1}$ is inconsistent with *Gaia* DR2.

Table 4: Known white dwarfs within 20 pc and potential 20 pc members without reliable five-parameter astrometric solutions. This includes systems in binaries where the companion is detected, as well as sources with incorrect five-parameter solutions that are omitted from the *Gaia* DR2 catalogue. Most systems have at least 2-parameter *Gaia* detections (with *Gaia* DR2 source IDs provided), but are noted where not detected at all. The reference column indicates the source of the quoted distance or parallax.

WD	Alt. name	<i>Gaia</i> DR2 ID	ϖ [mas]	D [pc]	Ref.	Note
0208-510	GJ 86 B	4937000898854436608	92.704 ± 0.045	10.787 ± 0.005	1	a
0413-077	40 Eri B	3195919254110817408	199.46 ± 0.32	5.014 ± 0.008	1	a
0454+620	PM J04586+6209	477633967143589760		21.6 ± 1.2	2	b
0553+053	G 99-47	3320184202856027776	125.0 ± 3.6	8.0 ± 0.2	3	
0727+482A	G 107-70A	975968340912004352	88.543 ± 0.066	11.294 ± 0.008	1	a, c
0727+482B	G 107-70B	975968340910692736	88.543 ± 0.066	11.294 ± 0.008	1	a, c
0736+053	Procyon B		284.56 ± 1.26	3.514 ± 0.016	4	d
1121+216	Ross 627	3978879594463069312	74.4 ± 2.8	13.4 ± 0.5	3	
1334+039	Wolf 489		121.4 ± 3.4	8.24 ± 0.23	3	e
1443+256	PM J14456+2527	1267487150183614976		17.5 ± 2.8	2	f
2140+078	NLTT 51908	2701893698904233216		25.1 ± 6.2	2	

References: (1) *Gaia* DR2 (companion), (2) Limoges et al. (2015), (3) van Altena et al. (1995), (4) van Leeuwen (2007).

Notes: (a) White dwarf does not have DR2 five-parameter astrometry, but known companion does. (b) A full *Gaia* astrometric solution is listed, but with a parallax of 11.36 ± 0.23 mas and ASTROMETRIC_EXCESS_NOISE > 1 mas. We do not rule out that it corresponds to this DA + dM system. (c) Three sources of similar magnitude and no *Gaia* astrometry at this position. (d) No *Gaia* detection due to saturation of Procyon A. (e) No *Gaia* detection, noting that the white dwarf has a ≈ 4 arcsec yr $^{-1}$ proper motion. (f) Detected with the established proper motion, but with a parallax of 1.44 ± 0.55 mas.

Table 5: Wide binaries identified in our 20 pc white dwarf sample.

J2015.5	Gaia DR2 ID	ϖ [mas]	μ_{Ra} [mas yr $^{-1}$]	μ_{Dec} [mas yr $^{-1}$]	G_{abs} [mag]	$G_{\text{BP}} - G_{\text{RP}}$	D_{\perp} [au]	Δv_{\perp} [km s $^{-1}$]	Note
015151.68+642549.4	518201792978858880	57.77 ± 0.02	+224.82 ± 0.03	-201.52 ± 0.03	12.7735 ± 0.0009	+0.256 ± 0.003	233.67 ± 0.09	1.244 ± 0.003	
015151.70+642602.9	518201792978856960	57.76 ± 0.03	+237.74 ± 0.04	-193.60 ± 0.04	9.2094 ± 0.0012	+2.345 ± 0.001			
021228.34-080417.9	2486388560866377856	59.88 ± 0.05	-609.29 ± 0.10	-448.00 ± 0.08	12.6241 ± 0.0019	+0.349 ± 0.009	60.31 ± 0.05	3.242 ± 0.012	1
021228.58-080417.4	2486388560866377728	59.83 ± 0.08	-604.92 ± 0.17	-488.69 ± 0.14	10.0750 ± 0.0031	+2.367 ± 0.004			
041629.95-591800.0	4678664766393827328	54.48 ± 0.05	-45.10 ± 0.08	-175.25 ± 0.09	11.1718 ± 0.0021	-0.139 ± 0.005	239.34 ± 0.22	0.705 ± 0.028	
041628.93-591810.4	4678664766394767616	54.71 ± 0.16	-48.30 ± 0.28	-167.80 ± 0.30	2.7540 ± 0.0072	+1.214 ± 0.004			
043115.25+585811.1	470826482635701376	181.28 ± 0.05	+1335.04 ± 0.08	-1947.63 ± 0.09	13.6445 ± 0.0007	+0.434 ± 0.005	56.39 ± 0.01	2.656 ± 0.043	
043114.12+585805.8	470826482635704064	180.42 ± 0.59	+1303.27 ± 2.05	-2043.85 ± 1.23	10.9795 ± 0.0074	+2.913 ± 0.005			
043645.16+270949.2	151650935831913216	57.49 ± 0.06	+227.51 ± 0.12	-148.43 ± 0.09	14.4231 ± 0.0023	+0.906 ± 0.005			
043648.51+270753.6	151650076838458112	57.10 ± 0.06	+232.87 ± 0.15	-148.14 ± 0.10	6.5012 ± 0.0027	+1.375 ± 0.005	2156.50 ± 2.21	0.444 ± 0.016	
074022.02-172457.6	5717278911884258176	109.22 ± 0.03	+1138.64 ± 0.04	-542.67 ± 0.04	13.1831 ± 0.0007	+0.336 ± 0.001	186.28 ± 0.05	0.654 ± 0.005	
074020.62-172454.2	5717278911884264576	109.05 ± 0.08	+1152.39 ± 0.11	-536.55 ± 0.12	14.1671 ± 0.0017	+4.392 ± 0.004			
074538.08-335525.3	5588614164276695424	64.78 ± 0.04	-276.18 ± 0.07	+1680.40 ± 0.08	15.3294 ± 0.0015	+1.403 ± 0.006	13437.15 ± 8.60	4.730 ± 0.035	2
074534.64-340954.7	5588607120530408832	65.11 ± 0.23	-220.65 ± 0.41	+1713.79 ± 0.44	4.2178 ± 0.0079	+0.773 ± 0.006			
075014.80+071121.3	3144837318276010624	54.93 ± 0.07	+211.54 ± 0.13	-1782.66 ± 0.08	15.3076 ± 0.0028	+1.413 ± 0.006	298.62 ± 0.38	0.689 ± 0.008	3
075015.56+071109.3	3144837112117580800	55.14 ± 0.06	+209.90 ± 0.11	-1790.48 ± 0.06	15.0671 ± 0.0025	+1.250 ± 0.006			
075356.28-252358.3	5602379190877207936	56.12 ± 0.08	-297.87 ± 0.13	+206.60 ± 0.26	14.7901 ± 0.0031	+1.128 ± 0.004	7123.83 ± 10.14	0.544 ± 0.022	
075410.54-251808.3	5602386058511578368	56.19 ± 0.03	-300.90 ± 0.04	+200.92 ± 0.05	7.8335 ± 0.0012	+1.797 ± 0.001			
104537.00-190654.4	3554395813252626048	53.13 ± 0.06	-1867.35 ± 0.10	-604.03 ± 0.07	14.0817 ± 0.0026	+0.792 ± 0.010			
104537.05-190701.0	3554395813252625920	53.16 ± 0.06	-1869.82 ± 0.09	-600.07 ± 0.07	8.9170 ± 0.0024	+1.979 ± 0.002	125.31 ± 0.14	0.416 ± 0.011	
113429.61-324949.6	3478127467639543296	104.74 ± 0.07	-701.62 ± 0.12	+828.82 ± 0.09	14.6595 ± 0.0018	+0.935 ± 0.005			
113428.66-324940.1	3478127463341507072	104.78 ± 0.05	-670.12 ± 0.08	+822.23 ± 0.05	5.8208 ± 0.0012	+1.002 ± 0.002	146.05 ± 0.10	1.456 ± 0.007	
133012.48-083436.8	363003578792473600	62.19 ± 0.09	-1111.14 ± 0.13	-472.38 ± 0.12	11.3450 ± 0.0030	-0.141 ± 0.004	8079.46 ± 11.11	0.270 ± 0.013	
133001.63-084232.8	3630015546177181952	62.14 ± 0.08	-1114.53 ± 0.15	-473.36 ± 0.12	11.6906 ± 0.0029	+3.079 ± 0.004			
134801.34+233448.4	1251824057289839744	84.27 ± 0.04	-1485.68 ± 0.06	+125.12 ± 0.05	14.9803 ± 0.0010	+1.284 ± 0.003			
134811.74+233650.6	1251824607045654016	84.18 ± 0.07	-1482.68 ± 0.12	+122.48 ± 0.08	13.0929 ± 0.0018	+3.545 ± 0.003	2232.50 ± 0.93	0.225 ± 0.007	
154729.47-375511.7	6009537829925128064	65.63 ± 0.05	-423.55 ± 0.10	-209.21 ± 0.06	12.1034 ± 0.0016	+0.090 ± 0.003	220.31 ± 0.15	0.695 ± 0.010	
154728.56-375502.0	6009538585839374336	65.53 ± 0.05	-415.24 ± 0.10	-214.03 ± 0.07	4.9011 ± 0.0017	+0.881 ± 0.003			
162333.94-391346.2	6018034958869558912	77.43 ± 0.07	+77.14 ± 0.15	+0.33 ± 0.11	10.4410 ± 0.0024	-0.376 ± 0.008			
162401.39-391134.7	6018047019138644480	77.47 ± 0.14	+74.15 ± 0.31	+3.67 ± 0.23	4.6395 ± 0.0044	+0.789 ± 0.008	4456.04 ± 4.05	0.275 ± 0.016	
163419.43+571027.5	1431176943768691328	67.32 ± 0.02	-1110.87 ± 0.05	+1199.40 ± 0.04	14.0024 ± 0.0009	+0.683 ± 0.003			
163418.21+571002.7	1431176943768690816	67.34 ± 0.05	-1113.61 ± 0.11	+1181.21 ± 0.10	10.6386 ± 0.0017	+2.934 ± 0.003	396.85 ± 0.14	1.295 ± 0.008	
192034.86-074002.6	4201781696994073472	95.25 ± 0.07	-61.28 ± 0.12	-161.77 ± 0.10	12.1651 ± 0.0018	+0.007 ± 0.010			
192033.39-073946.5	4201781696994082944	95.18 ± 0.08	-70.36 ± 0.12	-177.68 ± 0.11	10.8595 ± 0.0021	+2.567 ± 0.003	285.23 ± 0.22	0.912 ± 0.008	
205648.59-045043.0	6913810483611035776	61.75 ± 0.07	+776.36 ± 0.11	-222.94 ± 0.07	15.3161 ± 0.0024	+1.350 ± 0.005	242.90 ± 0.27	1.658 ± 0.018	
205649.36-045052.5	6913810483612308480	62.25 ± 0.10	+797.34 ± 0.16	-217.47 ± 0.13	9.6217 ± 0.0034	+2.708 ± 0.002			
210104.75-490627.8	6478328218869704192	74.89 ± 0.04	-286.96 ± 0.05	-226.36 ± 0.05	14.6478 ± 0.0012	+1.055 ± 0.003			
210106.95-490728.3	6478328150150225664	65.65 ± 0.49	-282.95 ± 0.63	-210.78 ± 0.64	11.0860 ± 0.0164	+2.812 ± 0.003	858.54 ± 0.46	1.091 ± 0.086	2

Table 5: continued.

J2015.5	<i>Gaia</i> DR2 ID	ϖ [mas]	μ_{Ra} [mas yr ⁻¹]	μ_{Dec} [mas yr ⁻¹]	G_{abs} [mag]	$G_{\text{BP}} - G_{\text{RP}}$	D_{\perp} [au]	Δv_{\perp} [km s ⁻¹]	Note
215139.93+591734.6	2202703050401536000	118.12 ± 0.02	-86.80 ± 0.04	-19.19 ± 0.04	14.7469 ± 0.0005	+1.060 ± 0.002	123.96 ± 0.02	1.207 ± 0.053	
215138.16+591740.0	2202703050388170880	123.06 ± 0.59	-79.19 ± 1.19	+10.52 ± 1.17	9.8337 ± 0.0105	+2.657 ± 0.003			
215738.28-510037.7	6558209044297239424	67.25 ± 0.03	-46.19 ± 0.04	-397.39 ± 0.04	13.6688 ± 0.0010	+0.554 ± 0.007	426.38 ± 0.18	1.456 ± 0.005	
215741.15-510028.1	6558208838138808576	67.29 ± 0.04	-35.50 ± 0.05	-379.72 ± 0.06	8.5356 ± 0.0015	+2.438 ± 0.003			
223035.20-751552.6	6357629089412187648	66.53 ± 0.05	+409.50 ± 0.09	-1827.90 ± 0.09	15.5757 ± 0.0017	+1.552 ± 0.007	1389.48 ± 0.99	0.185 ± 0.007	3
223041.65-751423.5	6357630601240673792	66.45 ± 0.04	+410.98 ± 0.08	-1825.78 ± 0.08	15.3136 ± 0.0016	+1.436 ± 0.006			
230959.27+550650.2	1996725077535283200	60.91 ± 0.04	+407.33 ± 0.06	+47.98 ± 0.06	14.5387 ± 0.0016	+0.902 ± 0.005	100.96 ± 0.07	0.471 ± 0.009	
230958.60+550648.0	1996725077535282944	61.04 ± 0.07	+409.09 ± 0.11	+42.18 ± 0.09	12.9382 ± 0.0027	+3.541 ± 0.008			

Notes: (1) Both the white dwarf and companionship are newly identified in this work. (2) Companion astrometry adversely affected by astrometric noise. (3) Wide double-degenerate system.

APPENDIX A:

We display fits of 15 *Gaia* sources with `ASTROMETRIC_EXCESS_NOISE` < 1 mas that were selected by the colour cuts of Equations (1–5) but not matched with known white dwarfs. In Fig. A1 we show the objects that we found in both Pan-STARRS and 2MASS. In Fig. A2 we display the remaining sources that are not in Pan-STARRS and hence we use *Gaia* and 2MASS photometry. In all cases we employ the *Gaia* parallax to constrain the surface gravity. We conclude that 9 objects are likely white dwarfs, which are catalogued in Table 1 and discussed in Section 2.2. The remaining 6 objects identified in Table 3 are more likely to be main-sequence stars with erroneous *Gaia* astrometry and/or colours (see Section 2.2).

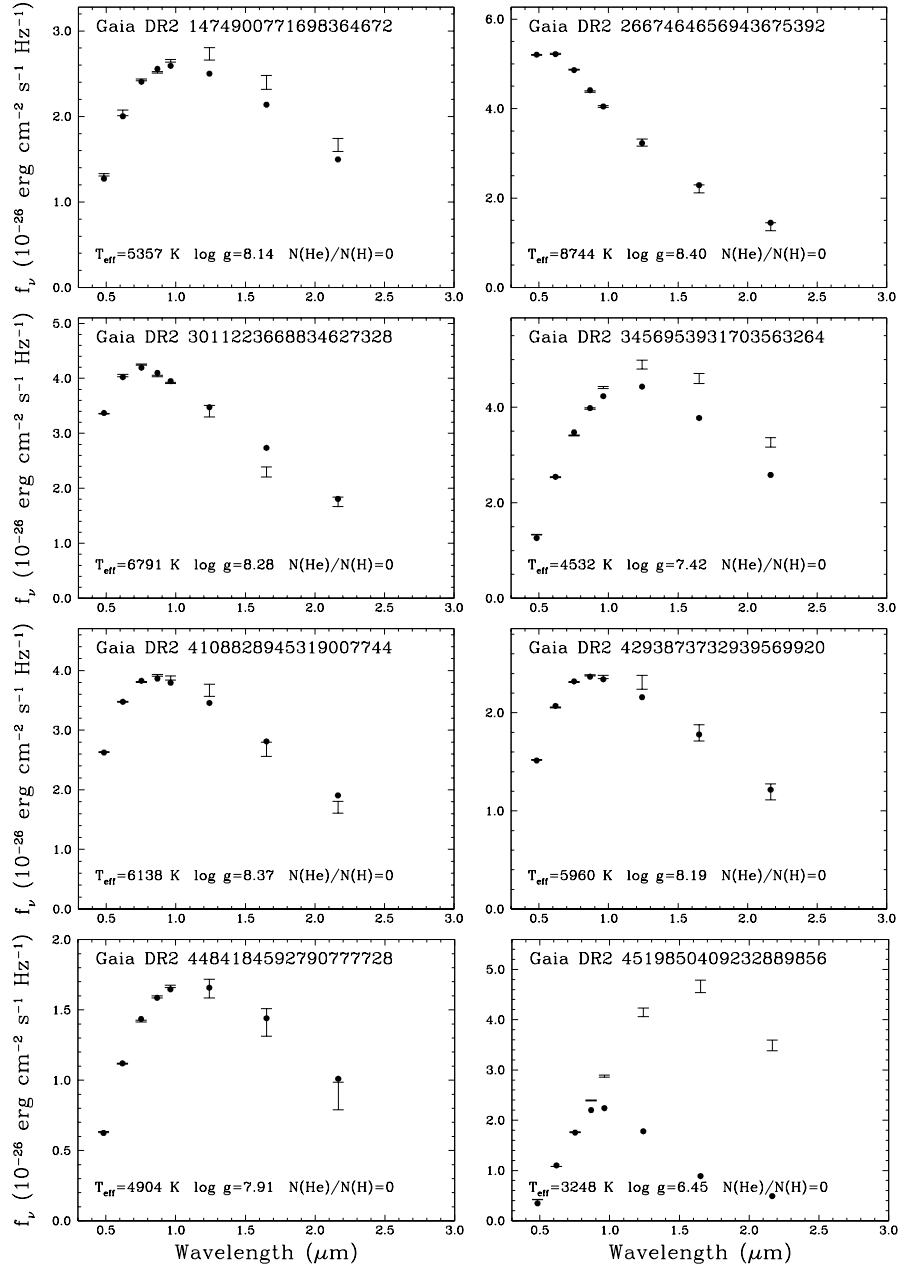


Figure A1. Fits to Pan-STARRS and 2MASS photometry (error bars) of white dwarf candidates using *Gaia* parallaxes and assuming pure-H model atmospheres (solid points). *Gaia* DR2 1474900771698364672, 3456953931703563264, and 4519850409232889856 are unlikely to be white dwarfs (see Table 3).

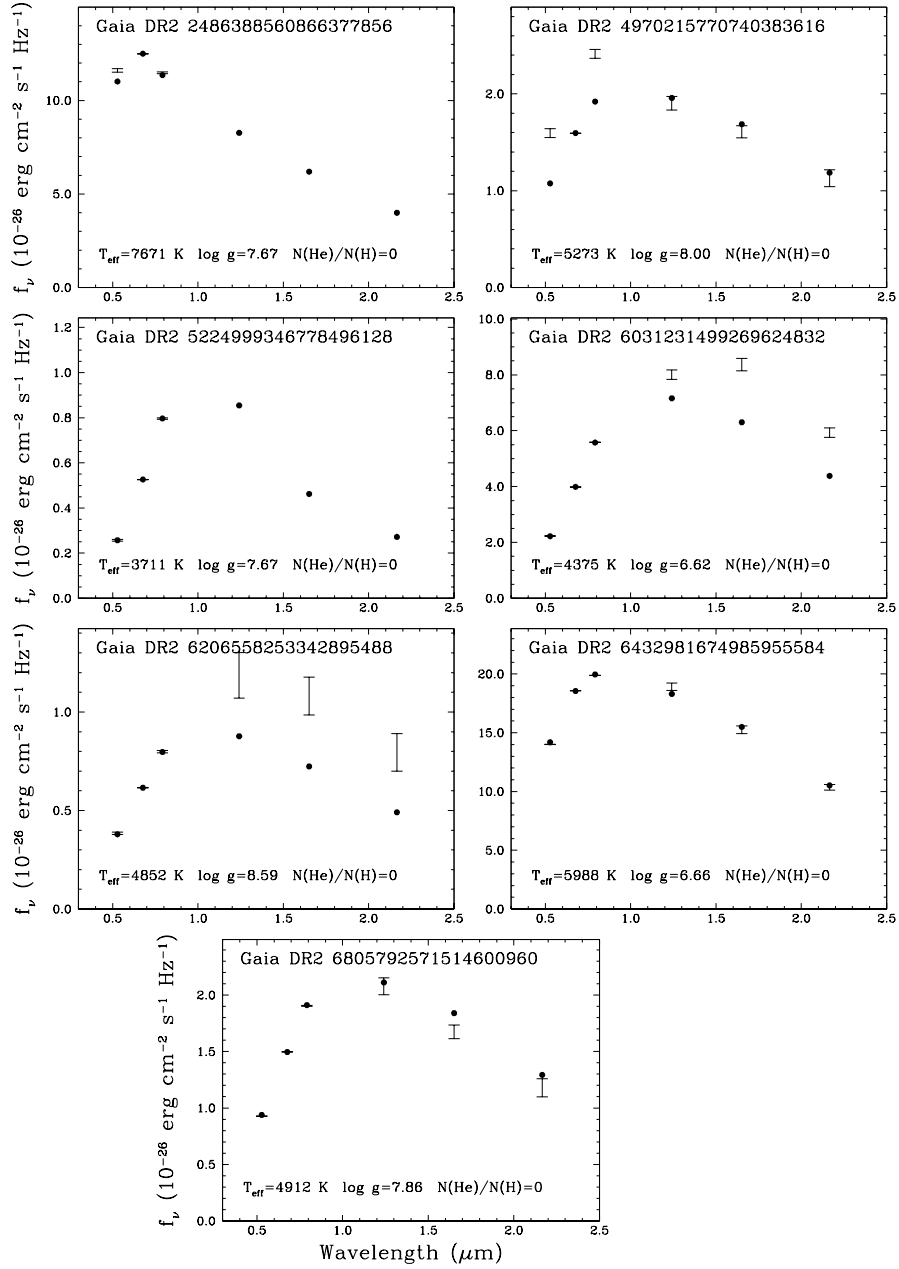


Figure A2. Fit to *Gaia* and 2MASS photometry (error bars) for white dwarf candidates using *Gaia* parallaxes and assuming pure-H model atmospheres (solid points). For two sources, *Gaia* DR2 2486388560866377856 and 5224999346778496128, no 2MASS counterpart was found and we fit *Gaia* data only. 6031231499269624832, 6206558253342895488, and 6432981674985955584 are unlikely to be white dwarfs (see Table 3).